Temporal evolution of jet induced scour depth in cohensionless granular beds and the phenomenological theory of turbulence

Fabián A. Bombardelli,[1, 3] Michele Palermo,[2] and Stefano Pagliara[2]

[1]Gerald T. and Lilian P. Orlob Endowed Professor, and [3]Corresponding author

Department of Civil and Environmental Engineering, University of California, Davis

2001 Ghausi Hall, One Shields Ave., Davis, CA 95616, USA.

E-mail: fabianbombardelli2@gmail.com, fabombardelli@ucdavis.edu

[2]Senior Researcher, and Professor, respectively

DESTEC-Department of Energy, Systems, Territory and Construction

Engineering, University of Pisa, Via Gabba 22, I-56100 Pisa, Italy.

In this work, we investigate the temporal evolution of the jet-driven scour depth in a pothole lying on a cohesionless granular bed, by using diverse approaches. First, we present new experiments which encompass cases with jet angles ranging from 45 to 90° from the horizontal, several initial water depths, and different particle sizes, supplementing experiments developed recently by the last two authors. In particular, we address relatively-large angles, mostly absent in previous analyses. Our results first confirm the existence of two very different stages in the scour process, essentially overlooked in datasets used to obtain the traditional formulas – *developing* and *developed* phases; they then provide unprecedented evidence of the very distinct behavior at 90°, characterized by a step-wise behavior. Second, after revisiting the rationale of a theory

for the equilibrium condition developed elsewhere by the first author and collaborator, we employ the existing and new datasets to determine the multiplicative constants embedded in the equilibrium scour formulas. Third, we present a novel theory for the temporal evolution of the scour depth of the pothole in the *developed* phase (but with good prediction capabilities in the *developing* phase as well). By invoking the conservation of mass of sediment in the pothole, in addition to the energy conservation within the pothole and the phenomenological theory of turbulence, we obtain ordinary differential equations which we solve by numerical means. We validate the theory using our new, and other datasets. Finally, we provide interesting interpretations of the scour process by using the results of the theory.

Key words: equilibrium scour depth, granular bed, phenomenological theory of turbulence, scour pothole.

I. INTRODUCTION

There are multiple practical situations addressed in the fields of hydrology, geomorphology, and planetary science which concern a jet plunging into a pool of water with a bottom constituted by a cohesionless granular material, and deal with the associated scour of such beds (Graf and Altinakar 1998). These situations include common potholes which occur downstream of hydraulic structures (Graf and Altinakar 1998), lead to crevasse lakes (USGS), are driven by head-cuts in drainage network evolution (Stein et al. 1993), form on consolidated deposits of nuclear waste (Hunter et al. 2013), take part during cleansing of gravel bars (Minh 1989), and were created on

Mars during Amazonian times (Wilson et al. 2004). Under those conditions, a turbulent cauldron initially appears within the pool of water; this cauldron then grows as it scours the pothole. The process continues until a dynamic equilibrium condition is attained between the flow and the granular bed (Fig. 1(a)). In spite of its pervasive appearance on Earth and other moons and planets, this phenomenon of scour still remains as one of the unsolved, classic topics of fluid mechanics (see Lee et al. 2016; Aamir and Ahmad 2016; Bates et al. 2016), since the times of Leonardo da Vinci and his famous drawings and sketches (Capra 2008).

Scour potholes may lead to severe practical consequences. For instance, in the streambed below an overflowing gate, or downstream of an outflow from a pipe, the evolving pothole may compromise the stability of the gate or the pipe (Graf and Altinakar 1998; Abt et al. 1984). Based on such risks and for almost one hundred years now, researchers from around the world have proposed a number of widely-used, important empirical formulas for the *equilibrium depth of the pothole* (see, for instance, Schoklitsch 1932; Mason and Arumugam 1985; Bormann and Julien 1991; Hoffmans and Verheij 1997). Formulations have been purportedly provided for a so-called "cylindrical," two-dimensional (2D) case, and for an "axisymmetric," three-dimensional (3D) counterpart. Most of these formulas have been obtained on grounds of dimensional analysis and heuristic arguments; they contain numerous free exponents that have been determined by fitting experimental results. In a few cases, one or more of those exponents has/have been determined semi-theoretically, as it is the case of, for example, the expressions of Ivanisevich Machado (1980), Bormann and Julien (1991), Stein et al. (1993), and Hoffmans (2009). To describe the state of the art regarding the formulas, Hoffmans

(2009) indicated the following: "…many of the existing scour relations are not universally applicable but dependent on the data that were used in the regression analyses. It is believed that a relation based on fundamental principles of physics, calibrated by using measured scour data, could overcome this problem…"

Mason and Arumugam (1985), Breusers and Raudkivi (1991), Hoffmans and Verheij (1997), and Hoffmans (2009) among others, have presented exhaustive compilations of formulas for the *equilibrium depth of the pothole*; we refer the reader to such compilations to avoid using space herein. It is apparent from those compilations that the formulas proposed so far are but special cases of the following generalized expression:

$$R = K\, q^{e_q}\, h^{e_h}\; g^{e_g}\, d^{e_d} \left(\frac{\rho}{\rho_s - \rho}\right)^{e_\rho} \tag{1}$$

where R is the sum of the scour depth, Δ, and the initial depth of the pool of water, D, $R = \Delta + D$ (see Fig. 1(a)); K is a multiplicative constant; q is the volumetric flow rate of the jet per unit thickness in a 2D set up (measured in the direction perpendicular to the paper in Fig. 1(a)) or the total discharge in a 3D condition; h is the head of the jet; g is the gravitational acceleration; d is the diameter of the grains of the bed; ρ is the density of water; ρ_s is the density of the grains of the bed; and e_q, e_h, e_g, e_d and e_ρ are exponents. In Table 1, we list the values of such exponents, either determined empirically by fitting different experimental results, obtained through semi-theoretical approaches, or set to zero from the start, by different researchers. From Table 1 it becomes evident that in some cases diverse researchers obtained widely dissimilar values of a given exponent.

A careful analysis of the available empirical and semi-empirical formulas for the equilibrium scour depth leads to the following observations (modified and extended from Bombardelli and Gioia 2005):

1) The formulas often lack dimensional homogeneity.
2) The formulas have often been predicated on limited experimental data in terms of number of jet angles and particle sizes explored.
3) The formulas have sometimes disregarded important parameters such as the diameter of the grains of the bed (see Hoffmans 1998, for $d_{90} > 0.0125$ m; Veronese 1937; and INCYTH 1982), which should in principle appear in the equations, at least in case of cohesionless granular beds. It is also clear that most formulas disregard the ratio of densities, with the exception of the expressions by Eggenberger and Muller (1944), and Bormann and Julien (1991). The acceleration of gravity does not appear explicitly either in most formulas; it could be argued that these variables are embedded in the multiplicative constant.
4) Most of the formulas do not provide much physical insight into the interaction between the granular bed and the turbulent cauldron.
5) The formulas do not specifically distinguish between 2D or 3D configurations. They might have had effects of lateral walls as well as scale issues.

To provide a fully-theoretical foundation to the scour phenomena, and in particular to offer insight into the interplay between production and dissipation of turbulence and the scour process, Bombardelli and Gioia (2005, 2006) and Gioia and Bombardelli (2005) pioneered a method based on the *phenomenological theory of turbulence* (hereafter denoted as PTT; Frisch 1995), thus predicting the *equilibrium scour depth* for 2D and 3D geometries. Their final formulas contain a multiplicative constant which cannot be determined from theoretical considerations; they are valid asymptotically under

conditions that are amply met in applications. In both cases, the formulas were validated through comparison of values of the exponents of the most widely-known expressions.

In addition to the analyses of the equilibrium scour depth, several works have been devoted to providing expressions for the *time evolution of the scour process*. These studies have similar characteristics of those related to the equilibrium depth in terms of reliance on experimental studies or semi-theoretical approaches (Stein et al. 1993). It was arguably Rouse (1940) the first who proposed that the scour depth induced by a jet grows with the logarithm of time. Although such statement would clearly lead to unbounded scour depths for very large times (which contradicts the empirical evidence and the verified notion of asymptotic equilibrium scour depth), this approach was followed by several renowned researchers (Stein et al. 1993). Laursen (1952), on the other hand, emphasized the existence of a "limiting extent of scour," and the decrease of the rate of scour as the turbulent cauldron is enlarged (Blaisdell et al. 1981). Blaisdell et al. (1981) discussed the very notion of equilibrium depth, and compared several formulations for the scour "velocity by which the scour depth increases" against data. They found that a hyperbolic function better describes the empirical evidence. Stein et al. (1993) developed further tests regarding the time evolution of the scour from overfall jets. They employed bed particle sizes in the range of coarse and fine sands, as well as cohesive sediment, and jets varying between 28 and 59° from the horizontal. Stein et al. (1993) concluded that both cohesive and non-cohesive sediment can be represented with a unique equation which they themselves developed by using the conservation of mass of sediment and an experimental expression for the jet-induced shear stress. Dey and Raikar (2007) undertook experiments with particle sizes in the range of sands and gravels, and validated

an exponential law with a particular time scale. More recently, Pagliara et al. (2008a, b), and Pagliara and Palermo (2008) conducted a series of experimental tests in order to analyze *both the scour process evolution and the equilibrium scour morphology due to plunging jets*. Based on the results obtained by Pagliara et al. (2006), Pagliara et al.'s experimental tests from 2008 focused on 3D scour geometries. In particular, Pagliara et al. (2008a) confirmed that the scour depth induced by a jet grows with the logarithm of time, but tends to an equilibrium value asymptotically. Pagliara et al. (2008b) very importantly introduced a quantitative criterion to distinguish among 2D and 3D cases. The criterion is as follows: 3D plunge pool scour involves the width parameter $\lambda=b_m/b$, in which b_m is the maximum extrapolated scour width, and b the channel width. For $\lambda < 1.5$ the scour plan shape is 3D, whereas it is nearly 2D for $\lambda > 3$. An intermediate behaviour should be expected for $1.5 < \lambda < 3$. Finally, Pagliara and Palermo (2008) investigated the 2D scour mechanism due to plunging jets in the presence of protection structures, testing empirical relations for the main geometric dimensions of the scour hole and ridge. Very importantly, Pagliara et al. (2006, 2008a) found that *there is a negligible effect of the jet condition (submerged/unsubmerged) on the maximum equilibrium scour depth* and on the features of the scour pothole. Further, they showed that there is a slight dependence on the jet nozzle geometry regarding that maximum depth.

A vast literature on the scour at *bridge piers* presents similar features as the cases of jet-induced scour. Very recently, Guo (2014) published a semi-theoretical solution to the problem employing the conservation of mass and an expression for the solid volumetric transport rate; numerous references therein describe the state of the art. Manes and

Brocchini (2015) in turn developed a theory by using the techniques introduced by Bombardelli and Gioia, which focuses only on the equilibrium condition.

Unlike the case of the equilibrium scour depth (Bombardelli and Gioia 2005, 2006; Gioia and Bombardelli 2006), there is no theory *solely based on conservation laws and the PTT* for the evolving scour depth induced by jets. After presenting novel experiments, we discuss the different elements of a new theory. Similar techniques to those developed herein can be applied to address the scour process of granular material surrounding abutments, as well as the cases of aerated jets, and scour of beds constituted by cohesive sediments.

II. EXPERIMENTAL INVESTIGATION OF TIME SCOUR EVOLUTION

A. Experimental setup, tests, and procedures

Experimental tests were developed at the Hydraulics Laboratory of the University of Pisa, Pisa, Italy. In Tables 2 and 3, we detail all tests used in this work, including those undertaken in 2006, 2008, and those especially obtained for this paper. These new tests were designed to provide a comprehensive picture of the scour phenomenon, including equilibrium and time-dependent tests.

Several of the new tests were conducted in order to simulate the cylindrical (2D) scour geometry at the *equilibrium condition* for jet angles (α, Fig. 1(a)) of 45, 60, 75 and 85°, and volumetric flow rates between 0.0025 m^3/s and 0.0045 m^3/s (line 5 in Table 2). These tests were performed in the same channel of Pagliara and Palermo (2008) (a 0.2-m wide and 6-m long channel) and used the same base granular material (d_{90}=11.1 mm, d_{50}=9.5 mm, and ρ_s=2,453 kg/m^3). Water was supplied through a movable circular pipe to

vary the location and angle (see Fig. 1(b)). This setup of using jets to obtain 2D scour configurations is a relatively-recent alternative as compared to old-fashion cylindrical tests, and contribute to reducing the overall model size (Pagliara et al., 2006).

For the 3D configuration, *scour-evolution* tests were undertaken involving a different cohesionless material; these tests were developed with a so-called "half model," in which a symmetry glassed plane was introduced in the flume to simulate half of the jet (line 6 in Table 2). Considering that a half-model arrangement was applied, the equivalent jet diameter for the full-model is $D^* = 2^{0.5} D_{test} = 0.0382$ m (see also Pagliara et al. 2008a), resulting in the same jet velocity in both the half- and full-models. In addition, the jet was issued about 2-3 mm from the glass wall, with minimal effect of such plane. In Pagliara et al. (2008a), a sketch of the "half-model" experimental set-up is presented. The jet angle was in this case of 90°, and the channel width was of 0.8 m. The channel bed material was characterized by the following properties: d_{50}=0.00745 m, d_{90}=0.0088 m, and ρ_s=2,468 kg/m^3. Test were conducted by varying water discharge from 0.00235 m^3/s to 0.00345 m^3/s. In Table 4, we report the scour depth evolution for tests with vertical jet arrangement (90°).

Prior to each test, the channel bed was carefully levelled and a transparent sheet with cell sizes of 0.5 cm x 0.5 cm was glued on the channel glass to help observe the evolution of the scour depth. Three different tailwater levels, D (Fig. 1(a)), ranging between 2.7 cm and 18.9 cm above the original channel bed level (set to ±1 mm), were tested, and they were kept constant during the experiments by adjusting a downstream sluice gate. Duration of all tests was of approximately one hour. After the equilibrium condition was attained, the main geometric features of the scour hole were measured by using a special

point gauge, including the maximum scour depth, Δ, the scour width, the pothole geometry, and the dune characteristics (Fig. 1(a)). This special point gauge, used previously by the authors, was equipped with a 40 mm circular plate at its lower end; therefore, the scour surface readings could be also taken in the presence of suspended particles and air bubbles in the scour hole. The overall accuracy of such point gauge is $\pm 0.5\ d_{50}$, where d_{50} is the sediment size for which 50% of material is finer. The longitudinal scour profiles were also determined from images and videos obtained by a fixed, high-resolution camera located in front of the channel (see also Pagliara et al. 2008a). The analysis of images and videos allowed for a careful estimation of bed profile at each instant, resulting in estimation errors ranging between two and three millimeters (i.e., almost equal to half mesh dimension).

In Fig. 2(a), we show a snapshot of an experimental test for α=60° (2D case) whereas in Fig. 2(b) we present the contour map and the 3D view of the equilibrium configuration for a test with a jet with α=60° (3D case).

B. Description of the physics of the scour time evolution for both 2D and 3D cases

The scour time evolution for all tests is characterized by two phases (Pagliara et al 2008a, b): an initial one, termed *developing* stage; and then the *developed* counterpart. The *developing* phase is very rapid; the scour process starts when the jet diffuses and impacts on the sediment surface (Stein et al. 1993; Hoffmans 2009), and afterwards a downstream (eventually surrounding) ridge starts to form. The so-called *developed* phase is characterized by an almost homothetic (i.e., proportional) expansion of both the scour

hole and the ridge. In Fig. 3, we include a schematic depicting the different steps pertaining to each phase. Snapshots of the *developing* and *developed* phases for a 3D configuration corresponding to a coarse bed, are presented in Figs. 4 and 5, respectively, for a jet angle of 45° (test especially developed for this work). Results of tests with fine material present similar features, albeit with a significant amount of sediment in suspension (see Pagliara et al. 2008a).

3D case. *For the 3D case*, in the first few seconds – less than 10 s for fine material and less than 5 s for the coarser tested material, when the ridge and dunes begin to form – the sediment transport is directed both longitudinally (x-direction) and laterally (y-direction). Then, sediment transport mostly occurs in the longitudinal direction for jet angles other than 90°. (The time difference stated above between coarse and fine material is due to the presence of more sediment in suspension in the latter case, which delays the formation of the pothole dunes (Dey and Sarkar 2006)). At this stage, the flow energy is not sufficient to transport all the scoured material, and therefore the accumulation in the ridge is enhanced. The process for the ridge evolves subsequently; in particular, the *upstream* ridge surface develops relatively fast (in less than 60 s for fine materials and less than 15 s for coarser materials), whereas the *downstream* part of the ridge requires a longer time to be shaped (up to approximately 90 s for fine materials and 25 s for coarser materials). It is worth noting that during the phase of ridge formation, a substantial increase of the scour pothole dimension takes place, and sediment particles are mainly transported downstream.

Once both the upstream and downstream surfaces are completely formed, the *developing* phase can be considered completed. Then, the *developed phase* takes place,

resulting in essentially *proportional enlargements of the scour hole and dune* (see Fig. 5 for coarser material). In particular, the dune starts shifting downstream and the scour hole surface expands both transversally and longitudinally, by increasing its depth. According to the jet angle and tailwater level (e.g., lower jet angles and high tailwaters; see Pagliara et al., 2008b) the scour pothole extension can be more prominent longitudinally than transversally. In any case, *the upstream scour origin does not shift significantly during the developed phase*.

Regarding the time evolution of the scour hole for larger angles in 3D, we corroborated that the larger the angle, the shorter the *developing* phase is, in agreement with the observations of Pagliara et al. (2008a). When the angle is relatively small, the average bed shear stress is naturally higher, and therefore the dune formation takes longer time because the transport of sediment dominates over depositional effects, especially in the very first instants of the scour process. In other words, during the *developing* phase, the downstream sediment deposit is partially flattened by the higher bed shear stress, resulting in a delayed dune developing process. It is worth noting that this mechanism is valid for both fine and coarse sediments; however, in the latter case, its effect is less prominent as coarser particles require higher shear stresses to be put into motion (Julien 2010). For higher jet angles, experimental evidence indicates that the scour depth after the first 3 seconds can reach about 30% of the final equilibrium depth.

3D case and jet angle of 90°. For α=90°, the phenomenology of the scour process is radically different than for other angles. Experimental tests showed that the amount of scour occurring in the very first seconds comprises more than 50% of the final, equilibrium depth. The *developing* phase in this case can last less than 20 s. *As a*

distinctive feature with respect to other jet angles, it was found that for 90° the scour depth evolution is characterized by the fact that sediment particles kept in suspension inside the scour pothole are removed from it in a non-monotonic fashion, thus resulting in a scour depth evolution by steps. This is shown in Fig. 6, which presents several snapshots of the evolution of the scour pothole for the 90° case, separated by only one second. It can be seen that whereas the same scour depth occurs at 4 and 5 seconds, there is a sudden increase at 6 seconds; then, the depth remains approximately constant from 6 to 7 seconds, suggesting that sediment particles abandon the pothole in a discontinuous way. This step-wise behavior becomes apparent in Fig. 7, in which the time evolution of the scour depths for all 90°-tests is presented. The length of the steps varies with the test. In Fig. 7, we have made the scour depth non-dimensional by the equivalent pipe diameter and we have used the same time scale of Pagliara et al. (2008a), i.e., we adopted the non-dimensional time $(g'\,d_{90})^{1/2}\,t/D^*$, with $T_r = D^*/(g'\,d_{90})^{1/2}$, where g' denotes the "reduced gravitational acceleration," equal to the product of gravity, the difference of the density of the sediment and water divided by the latter; and t is the time from the beginning of the test.

In Figs. 8 and 9, we present snapshots of the *developing* and *developed* phases, respectively, for a jet with and inclination of 90°, pertaining to tests with coarse material. The difference in the shape of the dune (and ridge), anticipated by Fig. 6, is striking. In this case, the symmetry of the scour process with the vertical axis is characteristic, fulfilling the canonical shape of vertical jets. It is also evident that the *developed* phase shows very modest increases of the scour depth, and a totally different shape for the ridge dunes.

2D case. *For the 2D case* (Figs. 10 and 11), the scour dynamics can be slightly different during the *developing* phase as opposed to the 3D case. In fact, the ridge only forms downstream of the scour hole; therefore, the evolution process can be slightly faster than for the 3D case, especially in the very first moments due to the absence of lateral sediment transport. This feature is evidenced in Fig. 10. During the first 2 s, after the jet impacts on the sediment bed, a rapid and generally symmetrical enlargement of the scour hole takes place up to the point in which the pothole reaches the channel walls (see Fig. 10(a)). This very initial phase is followed by a stage where the sediment transport is mainly directed downstream, as shown in Fig. 10(b). As for the 3D case, at this stage the jet energy is partially invested in lifting and keeping the bed sediment in suspension, resulting in the beginning of the downstream ridge formation. The upstream ridge surface is shaped in a very short time, in general slightly smaller than the 3D counterpart (see Fig. 10(c)). The dune formation limits the downstream sediment transport, causing an accumulation of sediment in correspondence with the ridge, and a reduction in the dynamics of the downstream dune surface shaping. At the same time, the scour-hole depth substantially increases and its longitudinal profile becomes more asymmetric. The *developing* phase ends when the downstream dune surface angle with respect to the horizontal becomes approximately equal to the wet angle of repose of the sediment material (generally for $t < 85$ s; see Fig. 10(d)). As a consequence, the total duration of the *developing* phase is comparable with that occurring for the 3D case under the same hydraulic conditions and jet configurations, even though the very initial phase of the process seems to be slightly faster for the 2D case (Pagliara et al. 2008a). The *developed phase* for the 2D case (Figs. 11) is characterized by a qualitative scour evolution behavior

which is rather similar to that of the 3D case, i.e., there exists a proportional expansion of both the scour hole and the downstream ridge, whereas the scour origin location does not shift significantly (Figs. 11(a)-(c)).

C. Transition time between developing and developed phases

We addressed the transition time between the *developing* and *developed* phases for the 3D case, as anticipated in Fig. 7. Therein, it can be seen that the transition time decreases for larger angles. The transition time was estimated by analyzing the time evolution and identifying the break in behavior in a semi-log plot (Pagliara et al., 2006). We were able to obtain an expression for such a variation as follows: $\log \tau_T = -0.02\,\alpha + 3.62$, with an R^2 value (defined in the Appendix) of 0.95, where τ_T is the transition time, and α is the jet angle. In Fig. 12, the time evolution of the scour process for diverse tests pertaining to different angles is presented in a semi-logarithmic scale. The differences in the behavior for distinct angles are apparent. The nomenclature of tests in Fig. 12 corresponds to that of Pagliara et al. (2008a), developed in Zurich, Switzerland: Its meaning is explained in the figure caption.

III. THEORETICAL EXPRESSION FOR THE EQUILIBRIUM SCOUR DEPTH

In this section, and for the sake of completeness, we briefly review the developments presented in Bombardelli and Gioia (2005, 2006), and Gioia and Bombardelli (2005) for the equilibrium conditions.

A. Use of the phenomenological theory of turbulence and jet energetics

Based on the two tenets of the PTT regarding the steady production of turbulent kinetic energy (TKE; Frisch 1995), it is possible to derive an expression for the rate of dissipation of turbulent energy per unit mass (denoted herein as ε) in terms of the velocity of the largest eddies (denoted by V) and of the size of the largest eddies (scaling with R); see Fig. 13(a) for its application to the scour problem. Those two tenets are as follows: (i) the TKE per unit mass is dictated by scales associated with the largest (energy-containing) eddies, being independent of viscosity; (ii) such TKE, introduced at a rate ε, transfers ("cascades") from large to small scales at the same rate ε until dissipation into internal energy takes place at the sufficiently-small scales. At the large scales, it holds from dimensional arguments that $\varepsilon \sim V^3/R$ (Lohse 1994), where the symbol "~" indicates "scales with;" for a generation of eddies of size l and velocity u_l, the eddy splitting and the transferring of TKE must be that $\varepsilon \sim u_l^3/l$, which together with $\varepsilon \sim V^3/R$ leads to the Kolmogorov scaling in the *inertial sub-range* (Pope 2000):

$$u_l \sim V \left(\frac{l}{R}\right)^{1/3} \tag{2}$$

This relation is valid for $l/\eta \gg 1$, where the η is the Kolmogorov length-scale ($\eta = \nu^{3/4} \varepsilon^{-1/4}$, with ν being the kinematic viscosity of water). The phenomenology above has been corroborated to occur at the inertial sub-range for a wide variety of flows (Saddoughi and Veeravalli 1994), but in the case of wall turbulence it requires further justification (Ali and Dey 2017). In spite of some theoretical inconsistencies presented elsewhere, *Ali and Dey (2017, 2018) concluded that the PTT (i.e., the scaling presented in Eq. (2)) still provides satisfactory results in wall-bounded flows*. Ali and Dey (2018) discussed numerous flows in which the PTT has allowed for predictions with accuracy,

such as the estimation of the equilibrium scour depth, the identification of the physical mechanisms which explain Nikuradse's diagram (Gioia and Chakraborty 2006), the link of the spectrum with the mean velocity profile (Gioia et al. 2010), the determination of scaling laws in sediment transport in water courses (Ali and Dey 2017), etc. By pointing out some limitations of alternative theories and the lack of a better, universal one, Ali and Dey (2018) highlighted the advantages of the PTT; thus, we follow Eq. (2) in our analysis.

The energetics of the turbulent cauldron dictates that the production of TKE is driven by the jet, whose power per unit thickness is P in 2D, or its power (also P) in 3D. This must equal the rate of dissipation of turbulent energy within the cauldron; we can thus write $P = \rho\ q\ g\ h = \varepsilon\ M$, valid for 2D and 3D under the use of the dual meaning of P explained above, and recalling that q represents the discharge per unit width in 2D, and the total discharge in 3D. $M \sim \rho\, R^2$ is the mass per unit thickness of cauldron in 2D, and $M \sim \rho\, R^3$ is the mass of the cauldron in 3D. It follows that $\varepsilon \sim q\ g\ h/R^2$ and $\varepsilon \sim q\ g\ h/R^3$ for the 2D and 3D configurations, respectively. Using $\varepsilon \sim V^3/R$, it is possible to find for the two conditions:

$$V \sim \left(\frac{q\ g\ h}{R}\right)^{1/3}; V \sim \left(\frac{q\ g\ h}{R^2}\right)^{1/3} \quad \text{(3a, b)}$$

Further, we surmise that the clouds of suspended sediment appearing in the experiments *do not* affect the energy transfer embedded in Eqs. (3).

B. Determination of the shear stress at the interface of the granular material

Next, we consider the surface of the pothole and seek to obtain a scaling expression for the shear stress exerted by the flow on that surface. We adopt a simple structure: We

assume that there exists a single turbulent layer governed by the phenomenological spectrum discussed above. From momentum-transfer and geometric considerations, it was shown in Gioia and Bombardelli (2002; see also Gioia and Chakraborty 2006 and Gioia et al. 2010) that the shear stress acting on a wetted surface tangent to the peaks of the grains at the surface of the pothole, S, is given by (Fig. 13(a)):

$$\tau = \rho \, |\overline{v_n \, v_t}| \sim \rho \, u_d \, V \tag{4}$$

where v_n and v_t are the fluctuating velocities normal and tangent to S, respectively, the overbar denotes time average, and u_d is the velocity scale of the eddy harbored within the roughness coves (Fig. 13(a)). Further, we assume that the lengthscale d is within the inertial subrange; thus, d follows the Kolmogorov scaling. Now, we may substitute V by Eqs. (3) and $u_d \sim V \left(\frac{d}{R}\right)^{1/3}$ in Eq. (4) to obtain:

$$\tau \sim \rho \, \frac{(q \; g \; h)^{2/3} \; d^{1/3}}{R} \; ; \tau \sim \rho \, \frac{(q \; g \; h)^{2/3} \; d^{1/3}}{R^{5/3}} \tag{5a, b}$$

which is valid for $\eta \ll d \ll R$. The results arrived at herein, derived from the use of the PTT and the jet energetics up to a multiplicative constant, do not employ empirical expressions to represent the bed shear stress.

C. Enforcement of the equilibrium condition

As the depth of the cauldron grows, the shear stress varies with $1/R$, and $1/R^{5/3}$, for 2D and 3D configurations, respectively; it decreases until it reaches a critical value τ_c, when the scour process ceases. Thus, the condition of equilibrium between the turbulent cauldron and the granular bed is $\tau=\tau_c$ (Yalin 1977; Raudkivi 1998). To obtain a scaling expression for the critical stress τ_c, we follow the experimental results by Shields on incipient motion of sediment for *relatively large* particle sizes (small to coarse sands;

Shields 1936; Yalin 1977; Julien 2010) and therefore establish that $\tau_c \sim (\rho_s - \rho)\ g\ d$. Imposing the equilibrium condition, and rearranging, the following scaling expressions for *R* are obtained:

$$R = K_0 \left(\frac{\rho}{\rho_s - \rho}\right) (q\ h)^{2/3}\ d^{-2/3} g^{-1/3} \tag{6a}$$

$$R = K_4 \left(\frac{\rho}{\rho_s - \rho}\right)^{3/5} (q\ h)^{2/5}\ d^{-2/5} g^{-1/5} \tag{6b}$$

One of the interesting aspects of this theory is that it predicts the same values for the exponents of *h* and *q* (see Bombardelli and Jha 2011).

IV. THEORETICAL/NUMERICAL MODELS FOR THE TIME EVOLUTION OF THE SCOUR DEPTH IN THE DEVELOPED STAGE

In this section, we present an unprecedented theory for the temporal evolution of scour. We assume that Eqs. (5) for the shear stress, and the momentum transfer mechanism explained in Fig. 13(a), hold true *at all times* in the scour process.

We start the analysis for a 2D configuration. As a consequence of the action of the shear stress, grains abandon the cohesionless bed at a rate q_s per unit width of pothole. We follow our empirical evidence *in the developed* phase and argue that the evolution of the pothole can be approximated as homothetic through a circumference whose center is always located at the free surface, and whose distance from the initial bed elevation is Δ (Fig. 13(b)). Naturally, this assumption does not allow for the representation of the sediment which is removed from the pothole and is deposited at both sides, as it is observed in the experiments (see for instance Figs. 10 and 11); this assumption ensures that the problem is mathematically tractable. The area of the scoured material scales with the product of the scour depth Δ, and of the length *r*, i.e., $A \sim \Delta\, r$ (recall that the area of

an ellipse is π times the product of the two axes of the ellipse). In order to obtain an expression for *r*, we can write that $r^2 + D^2 = R^2 = (D + \Delta)^2$. From this, it is possible to obtain that $r^2 = 2\,\Delta\,D + \Delta^2$. Further, we assume that the first term of last expression dominates or, equivalently, that $\frac{\Delta}{D} \ll 1$. This assumption is accurate during the initial stages of the scour process and becomes less so close to its end; however, we believe that it constitutes a good scaling approximation which is of the same order of magnitude than neglecting the details of the geometry of the scour pothole. Therefore, it is possible to find that $r \sim \sqrt{\Delta\,D}$ and $A \sim \Delta^{3/2}\sqrt{D}$.

In addition, the rate of material removal from the bed (per unit width; [m^2/s]) scales as: $q_s \sim \frac{dA}{dt} \sim \frac{d\,(\Delta^{\frac{3}{2}}\,D^{\frac{1}{2}})}{dt} = D^{1/2}\,\frac{d\,(\Delta^{\frac{3}{2}})}{dt} = \frac{3}{2}\,D^{1/2}\,\Delta^{1/2}\,\frac{d\Delta}{dt}$, where we have made use of the fact that the initial water depth remains constant in time. In other words, $q_s \sim D^{1/2}\,\Delta^{1/2}\,\frac{d\Delta}{dt}$. (In this last result, we considered that the difference in density between the sediment in the bed and that transported downstream can be included in the multiplicative constant; see Guo 2014.)

On the other hand, the amount of scoured material has to scale with the excess of shear stress over the critical shear stress, following usual formulas of sediment transport (Yalin 1977; Julien 2010; Parker 2004; García 2008; Foster et al. 1977; Stein et al. 1993):

$$\frac{q_s}{\sqrt{\frac{(\rho_S - \rho)}{\rho}\,g\,d^3}} \sim \left(\frac{\tau}{\tau_c} - 1\right)^{m_1} \tag{7}$$

We accept that exponent m_1 varies from 1 for cohesive sediment (not the scope of this work), to the range 1.5-2 for non-cohesive sediment (Yalin 1977; Julien 2010; Parker 2004; García 2008). Considering the factors in Eq. (7), the expression for the shear stress is taken from Eq. (5a) and the critical shear stress is provided by Shields work; therefore:

$$\frac{D^{1/2}\ \Delta^{1/2}\frac{d\Delta}{dt}}{\sqrt{\frac{(\rho_S-\rho)}{\rho}\ g\ d^3}} \sim \left(\frac{K_1\ \rho\ \frac{(q\ g\ h)^{2/3}\ d^{1/3}}{R}}{K_2\ (\rho_S-\rho)\ g\ d} - 1\right)^{m_1} \tag{8}$$

or:

$$\frac{d\Delta}{dt} = K_3\sqrt{\frac{(\rho_S-\rho)\ g\ d^3}{\rho\ D}}\ \frac{1}{\Delta^{1/2}}\ \left(\frac{K_1\ \rho\ \frac{(q\ g\ h)^{2/3}\ d^{1/3}}{R}}{K_2\ (\rho_S-\rho)\ g\ d} - 1\right)^{m_1} \tag{9}$$

where K_1 and K_2 are multiplicative constants for the shear stress and for the critical shear stress, respectively. K_3 is the constant for the rate of change of the scour depth. Under equilibrium conditions, the two shear stresses embedded in (9) become equal, giving a null rate of change, and $R_{eq} = D + \Delta_{eq}$. For that condition:

$$\rho\ (q\ g\ h)^{2/3}\ d^{1/3} = \frac{K_2}{K_1} R_{eq}\ (\rho_s - \rho)\ g\ d \tag{10}$$

Thus, replacing in (9):

$$\frac{d\Delta}{dt} = K_3\sqrt{\frac{(\rho_S-\rho)\ g\ d^3}{\rho\ D}}\ \frac{1}{\Delta^{1/2}}\ \left(\frac{R_{eq}}{R} - 1\right)^{m_1} \tag{11}$$

For a 3D configuration, the procedure is very similar. We start by considering the rate of volumetric transport of sediment out of the pothole, with the scoured *volume* given by $Vol \sim A\ r \sim \Delta\ \ r^2 \sim \Delta^2\ D$. It is immediate to write for q_s ([m^3/s]) that $q_s \sim \frac{dVol}{dt} \sim \frac{d\left(\Delta^2\ D\right)}{dt} = 2\ D\ \Delta\ \frac{d\Delta}{dt}$ and:

$$\frac{q_s}{\sqrt{\frac{(\rho_S-\rho)}{\rho}\ g\ d^5}} \sim \left(\frac{\tau}{\tau_c} - 1\right)^{m_2} \tag{12}$$

Following the same steps and using Eq. (5b), we can obtain:

$$\frac{d\Delta}{dt} = K_7\sqrt{\frac{(\rho_S-\rho)\ g\ d^5}{\rho\ D^2}}\ \frac{1}{\Delta}\ \left(\frac{K_5\ \rho\ \frac{(q\ g\ h)^{2/3}\ d^{1/3}}{R^{5/3}}}{K_6\ (\rho_S-\rho)\ g\ d} - 1\right)^{m_2} \tag{13}$$

After imposing equilibrium conditions:

$$\frac{d\Delta}{dt} = K_7 \sqrt{\frac{(\rho_s - \rho)\, g\, d^5}{\rho\, D^2}}\, \frac{1}{\Delta} \left[\left(\frac{R_{eq}}{R}\right)^{5/3} - 1\right]^{m_2} \quad (14)$$

Eqs. (11) and (14) constitute the ordinary differential equations (ODEs) of the time-dependent problem *for the developed stage*, represented mathematically as an initial value problem (IVP). *The initial condition* can be extracted from the experimental data*, at the transition point between the two phases*, following the hypothesis included in the model development.

Very importantly, *Eq. (11) is a function solely of the exponent* m_1 *and the multiplicative constant* K_3*; Eq. (14) depends on the exponent* m_2 *and the constant* K_7*.* In other words, if the exponents are fixed, the ODEs depend on just the multiplicative constants! The remaining variables in the equations are readily available from the tests. Constants K_1, K_2 and K_5, K_6 are *auxiliary* variables, *which do not need to be determined to solve the ODEs.* The solutions to the ODEs were implemented in numerical codes in `Matlab`, by using a simple Euler method. Grid-independence tests were developed to ensure numerical accuracy. Verification of the codes were developed using other languages as well.

V. THEORY VALIDATION

A. Determination of the multiplicative constants for the *equilibrium* conditions

Datasets included in Tables 2 to 4 were employed to obtain constants K_0 and K_4 of Eqs. (6). In Fig. 14, we graphically compared the *measured* values of the scour depth versus the *calculated* scour depths by using a value of the corresponding K equal to one in Eqs. (6); the slope of the regression line (obtained with the Least Squares Method) gives the values of multiplicative constants for the equilibrium condition, for 2D and 3D

configurations. From our new experiments, the velocity of the jet, v_{jet}, is available; therefore, the head of the jet was obtained as $h = \frac{v_{jet}^2}{2\,g}$. In the 2D case, when the symmetrical configuration was used, the discharge per unit width was determined as $q = 2\,Q_{jet}/D^*$ (half model) and $q = Q_{jet}/D^*$ for the full model. For the 3D configuration, the values of $2\,Q_{jet}$ and Q_{jet}, under the two conditions, were employed, respectively.

The results of the analysis indicate that the corresponding constants are **0.29** and **0.49** for the 2D and 3D configurations, respectively. These values were rounded to **0.3** and **0.5**, with minimal loss of accuracy.

B. Validation of the formula for the equilibrium conditions with other laboratory and field datasets

Once their respective constants have been determined, we employed several datasets published elsewhere in order to validate our expressions for the equilibrium scour depth. In Fig. 15, we show comparisons of experimental data points of Veronese (1937), with computations obtained with Eq. (6b), corresponding to a 3D configuration and a value of the constant equal to 0.5; in addition, a 30% variation interval was included. It can be seen that the equation for a 3D configuration predicts very closely the data, with a value of the proportionality constant determined from our tests (i.e., it was not calibrated).

We also validated the 3D equilibrium formula with some *field* cases, obtaining important success without tuning any coefficient (not shown herein). More work is needed in this regard, and this issue of potential scale effects will be discussed in a future paper.

C. Validation of the expressions for the time-dependent scour process

Inspired by the work by Stein et al. (1993), we checked that model solutions resembled the typical "S curve" of their Fig. 2; our solutions did not use any ad-hoc, empirical formulations for the shear stress; *only conservation laws and the PTT*. The behavior of our curves is in qualitative agreement with that of Stein et al. (1993), with the same variations of the curves with respect to the multiplicative constants and the exponents.

The next step was to compare the prediction of the models against measurements developed by Pagliara et al. (2008a) in Zurich; we started with the developed phase, where the model strictly holds. We set both exponents m_1 and m_2 to 1.5, following Foster et al. (1977); then, we developed a *calibration* of the multiplicative constants for 2D and 3D, beginning for 45°, using some of those datasets. Initial conditions were taken at the beginning of the developed phase. Then, we *validated* the selections of the multiplicative constants by comparing against others of those Zurich datasets. It is worth mentioning here that after the calibration-validation process undertaken for 45°*, the same multiplicative constants were used for 60 and 90°, in order to have a solid predictive tool*. Finally, we validated our models for the entire scour process.

Results for the *2D configuration* are presented on Figs. 16: Whereas the calibration results for 45° are introduced in tile (a), those of the validation for the same angle are depicted in tile (b). It can be seen that the theoretical/numerical model predicts the first selected tests with good accuracy (root mean square error, RMSE, values smaller than 0.0192 in the relative scour depth, which is very good within the scour and sediment-transport fields) with a determined multiplicative constant, K_3=**8** and m_1=1.5. (After

applying a Least Square Error algorithm, we rounded the final value.) Error bars of 2% of the dimensionless scour depth (estimated from the experimental results) have been included in the comparisons. Furthermore, the predictions agree with data for both submerged/unsubmerged jets. When the model results are compared against other Zurich tests in tile (b), it is possible to see that the model performs satisfactorily (RMSE=0.0643 for Test 59 and 0.173 for Test 56) *for the same constant and exponent*. Scour-depth values obtained for Test 56 show a sudden variation in the rate of change of the scour process; we do not have a clear explanation for this behavior. The predictions of the scour depth in tile b) are larger than those observed, showing faster scour rates; we suggest herein that this could be explained by the fact that the theory does not incorporate in its current version the effects of the cloud of suspended sediment seen in many experiments. Thus, the theory does not account for the energy invested in keeping the sediment in suspension, and therefore the larger scour depth is the result of a larger shear stress (in the model) which becomes important in a few tests. Further, this occurrence was experimentally suggested by conducting special tests in which the suspended material was removed during the scour process from the pothole: A general enlargement was noticed with respect to the case in which the granular material was left rotating within the scour hole. This effect might be exacerbated by the volumetric flow rate of the test.

In Fig. 17, computations for 60° for the *2D arrangement* are compared against data. *The same parameters determined in the calibration phase for 45° (i.e., K_3=**8** and m_1=1.5*) *were used herein*. It can be seen that the model predicts the experimental tests with good accuracy (RMSE values smaller than 0.0291).

Results for the *3D configuration* are presented in Figs. 18, for 45°; again, we separated between calibration and validation. The obtained multiplicative constant for 3D cases in tile (a), after the application of the Least Square Method and rounding, is K_7=**80**, for m_2=1.5. The model again predicts the experimental data for the developed phase with good accuracy (RMSE values smaller than 0.0579). In tile (b), we used the same values of K_7 and m_2 above, and the comparisons indicate good agreement as well, with RMSE values smaller than 0.0529, except Test 20 (RMSE=0.105). Very interestingly, for the validation tests (Fig. 18(b)), the *model predictions are below the observed values of scour depth*, which is opposite to what was observed for 2D cases. We suggest that this is the result of the flow physics in the 3D configuration. As stated above, in the 3D scour evolution the sediment is also transported in the transverse direction, forming a dune which occupies the entire ridge. This effect is not considered in the theory, and thus there is no limitation for the homothetic growth. Thus, the dune in the laboratory experiment offers a confinement which is not present in the theory, leading to larger laboratory values of the shear stress and of the scour depth. This effect, again, seems to be important only in some tests.

For tests with 60° in a 3D configuration, we developed simulations with the same values of the multiplicative constant and exponent (i.e., K_7=**80**, for m_2=1.5). The agreement was found to be very satisfactory (not shown herein) with RMSE values smaller than 0.053.

In Fig. 19, the calculations for tests pertaining to 90° in a 3D configuration, are shown. Again, we conducted them with the same values of the multiplicative constant and exponent (i.e., K_7=**80**, for m_2=1.5). Although the theoretical model was not intended

in the current form to capture the step-wise behavior described in the previous sections of the paper, the solutions are able to predict well the general evolution of the data. In some tests, the model over-predicts the rate of change of the scour depth. Indeed, further tests will provide insight into the details of the behavior, but the level of prediction is remarkable given that the same values of the model parameters have been used.

Although the comparisons against data this far have been obtained with 4 to 7 data points per test, when all points are included a single plot predicted scour depth versus measured scour depth, it is possible to see that the vast majority of points is within 10% of variation, and *all* are within 30%, indicating a very good agreement (Fig. 20).

The models can in principle offer insight for the entire scour evolution – i.e., for both *developing* and *developed* phases. In Fig. 21, we provide a quick comparison against experimental results by Stein et al. (1993), via the use of the same multiplicative constant, and m_1=1.5 of the 2D configuration. The comparison with the experiments of Stein et al. (1993) is rather difficult because the authors do not specify the original water depth. In our simulations, we performed an estimation of such water depth, obtaining accurate results in the model predictions for tests presented in their paper. The model is able to produce the shape of the experimental data.

VI. CONCLUSIONS

In this paper, we addressed the time-dependent scour depth induced by jets over *non-cohesive*, granular material, having the equilibrium condition as a particular case. In first

place, we presented careful experimental tests regarding the scour evolution under a considerable range of jet angles (from the horizontal) including the much less frequent case of 90°. From those tests, our results corroborated the classification recently put forward elsewhere regarding the existence of two clear phases: *Developing* and *developed* phases, and highlighted the homothetic nature of the latter. This last piece of information proved to be crucial for the validation process of the theory. Further, new evidence regarding the unique dynamics pertaining to an angle of 90° was provided, indicating a step-wise progression of the scour depth, and a very fast dynamics in the initial stages of the process. The dynamics for 90° thus differ substantially from that of other angles. The transition time between the two stages was characterized with a linear relation of the logarithm of the transition time and the jet angle.

Second, for the first time to the best of our knowledge, *the subject has been fully approached via the PTT and conservation laws in a novel theory*, up to a multiplicative constant. In spite of purported shortcomings highlighted elsewhere, the phenomenological theory appears once again as a very useful tool for understanding diverse aspects of hydraulics, as remarked by a recent review, until more sophisticated theories become available. Data from our and others' work allowed us to obtain the multiplicative constant for the equilibrium scour depth. For the time evolution, a simple mass balance was used in addition to the PTT and a simplified pothole shape, to provide an unprecedented, *unified picture* conducive to the theoretical analysis of the problem for 2D and axi-symmetrical geometries. The models are rigorously valid during the *developed* phase, where the homothetic behavior and the adopted shape strictly hold. A couple of ODEs was obtained, which can be solved numerically with standard methods.

Each ODE very nicely *depends on a multiplicative constant and an exponent*; the exponent was fixed at 1.5, and each constant was obtained via comparison against our own experiments for 2D and 3D. Since our experimental results correspond to rather small sizes, the validity of the developed equations for diverse *(large) scales* is left for future work.

It was shown that the theoretical/numerical models predict closely the experimental data with both submerged and unsubmerged conditions, for the *developed* phase of our experimental data. Further, the models successfully provide insight *for all stages* of the scour process.

ACKNOWLEDGMENTS

We thank very much Profs. Gustavo Gioia, and Pinaki Chakraborty, from the Okinawa Institute of Science and Technology (OIST), Japan, for many illuminating discussions on the subject. We also thank Ms. Amanda Poole for her work on very early stages of the project. Finally, we thank the technicians of the hydraulics laboratory of the University of Pisa, Mr. Nicola Bruni, Mr. Antonio Cecchi, Mr. Alessandro Michelotti, and Mr. Vincenzo Pennabea for their help in building the experimental apparatus.

APPENDIX: MESURES OF ERROR FOR MODEL VALIDATION

The quantification of error was undertaken using well known metrics, as described here. R^2 is the coefficient of determination, defined as:

$$R^2 = 1 - \frac{\sum_{i=1}^{N}(O_i - M_i)^2}{\sum_{i=1}^{N}(O_i - \bar{O})^2} \quad \text{(A1)}$$

where O and M indicate the observed and modeled values, respectively; the overbar represents the averaged values; and N is the number of points used. In turn, the RMSE is defined as:

$$RMSE = \left\{\frac{[\sum_{i=1}^{N}(O_i - M_i)^2]}{N}\right\}^{1/2} \quad \text{(A2)}$$

REFERENCES

Aamir, M., and Ahmad, Z., "Review of literature on local scour under plane turbulent wall jets," Physics of Fluids 28, 105102 (2016).

Abt, S. R., Kloberdanz, R. L., and Mendoza, C., "Unified culvert scour determination," Journal of Hydraulic Engineering ASCE 110, 1475 (1984).

Aderibigbe, O. O., and Rajaratnam, N., "Erosion of loose beds by submerged circular impinging vertical turbulent jets," Journal of Hydraulic Research, IAHR 34, 19 (1996).

Ali, S. Z., and Dey, S., "Origin of the scaling laws of sediment transport," Proceedings Royal Society London Ser. A 473(2197), 20160785 (2017).

Ali, S. Z., and Dey, S., "Impact of phenomenological theory of turbulence on pragmatic approach to fluvial hydraulics," Physics of Fluids 30, 045105 (2018).

Bates, M., Andreini, N., and Ancey, C., "Basal entrainment by Newtonian gravity-driven flows," Physics of Fluids 28, 053101 (2016).

Blaisdell, F. W., Anderson, C. L., and Hebaus, G. G., "Ultimate dimensions of local scour," Journal of the Hydraulics Division, ASCE 107(HY3), 327-337 (1981).

Bombardelli, F. A., and Gioia, G., "Towards a theoretical model for scour phenomena." In Proc. RCEM 2005, 4th IAHR Symposium on River, Coastal, and Estuarine

Morphodynamics, Urbana, IL, USA, G. Parker, and M. García (Eds.), Vol. 2, 931-936 (2005).

Bombardelli, F. A., and Gioia, G., "Scouring of granular beds by jet-driven axisymmetric turbulent cauldrons," Physics of Fluids 18, 088101 (2006).

Bombardelli, F. A., and Jha, S. K., "Discussion of 'Closure problem to jet scour' by G. J. C. M. Hoffmans," Journal of Hydraulic Research, IAHR 49(2), 277-279 (2011).

Bormann, N. E., and Julien, P. Y., "Scour downstream of grade-control structures," Journal of Hydraulic Engineering, ASCE 117(5), 579-594 (1991).

Breusers, H. N. C., and Raudkivi, A. J., *Scouring: Hydraulic Structures Design Manual Series* (Balkema, The Netherlands, 1991).

Capra, F., *The science of Leonardo: Inside the mind of the great genius of the Renaissance* (Anchor Books, New York, 2008).

Chee, S. P., and Padiyar, P. V., "Erosion at the base of flip buckets," Engineering Journal, Institute of Canada 52(111), 22-24 (1969).

Chee S. P., and Kung T., "Piletas de derrubio autoformadas," in Proc. 6th IAHR Latin American Congress, Bogotá, Colombia (1974).

Dey, S., and Raikar, R. V., "Scour below a high vertical drop," Journal of Hydraulic Engineering, ASCE 133(5), 564-568 (2007).

Dey, S., and Sarkar, A., "Scour downstream of an apron due to submerged horizontal jets," Journal of Hydraulic Engineering, ASCE 132(3), 246-257 (2006).

Ervine, D. A., Falvey, H. T., and Withers, W., "Pressure fluctuations on plunge pool floors," Journal of Hydraulic Research, IAHR 35(2), 257-279 (1997).

Foster, G. R., Meyer, L. D., and Onstad, C. A., "An erosion equation derived from basic erosion principles," Transactions ASAE 20(4), 678-682.

Franke, P. G., "L'affouillement: mecanisme et forms," Oesterreichische Wasserwirtschaft (1960).

Frisch, U., *Turbulence* (Cambridge University Press, Cambridge, 1995).

García, M. H., *Sedimentation engineering: processes, measurements, modeling, and practice*. *Manual 110* (American Society of Civil Engineers, Reston, VA, USA)

Gioia, G., and Bombardelli, F. A., "Scaling and similarity in rough channel flows," Physical Review Letters 88, 014501 (2002).

Gioia, G., and Bombardelli, F. A., "Localized turbulent flows on scouring granular beds," Physical Review Letters 95, 014501 (2005).

Gioia, G., and Chakraborty, P., "Turbulent friction in rough pipes and the energy spectrum of the phenomenological theory," Physical Review Letters 96, 044502 (2006).

Gioia, G., Guttenberg, N., Goldenfeld, N., and Chakraborty, P., "Spectral theory of the turbulent mean-velocity profile," Physical Review Letters 105, 184501 (2010).

Graf, W. H., and Altinakar, M., *Fluvial Hydraulics* (John Wiley and Sons, Chichester, UK., 1998).

Guo, J., "Semi-analytical model for temporal clearwater scour at prototype piers," Journal of Hydraulic Research, IAHR 52(3), 366-374 (2014).

Hartung, F., "Ursache und verhutung der stauraumverlandung bei talsperren," Wasserwirtschaft 1, 3-13 (1959).

Hoffmans, G. J. C. M., and Verheij, H. J., *Scour manual* (Balkema, The Netherlands, 1997).

Hoffmans, G. J. C. M., "Jet scour in equilibrium phase," Journal of Hydraulic Engineering, ASCE 124(4), 430-437 (1998).

Hoffmans, G. J. C. M., "Closure problem to jet scour," Journal of Hydraulic Research, IAHR 47 (1), 100-109 (2009).

Hunter, T. N., Peakall, J., Unsworth, T. J., Acun, M. H., Keevil, G., Rice, H., and Biggs, S., "The influence of system scale on impinging jet sediment erosion: Observed using novel and standard measurement techniques," Chemical Engineering Research and Design 91, 722-734 (2013).

INCYTH-LHA, *Estudio sobre modelo del aliviadero de la presa Casa de Piedra. Informe final*, Report LHA-INA, Ezeiza, Argentina (1982). (In Spanish.)

Ivanisevich Machado, L., "Formulas to calculate the scour limit on granular or rock beds." In Proc. XIII National Workshop on large dams, Rio de Janeiro, 35-52 (1980).

Julien, P. Y., *Erosion and sedimentation* (Cambridge University Press, Second Edition, 2010).

Kotoulas, D., *Das kolkproblem unter besonderer berucksichtigung der faktoren zeit und geschiebemischung in rahmen der wildbachverbauung* Dissertation, Prom. 3983, Technischen Hochschule Zurich.

Laursen, E. M., "Observations on the nature of scour," in Proc. 5th Hydraulic Conference, University of Iowa, Iowa City, Iowa, Iowa Bul. 34, 179-197 (1952).

Lee, C-H., Low, Y. M., and Chiew, Y. M., "Multi-dimensional rheology-based two-phase model for sediment transport and applications to sheet flow and pipeline scour," Physics of Fluids 28, 053305 (2016).

Lohse, D., "Crossover from high to low Reynolds number turbulence," Physical Review Letters 73, 3223-3226 (1994).

Manes, C., and Brocchini, M., "Local scour around structures and the phenomenology of turbulence," Journal of Fluid Mechanics 779, 309-324 (2015).

Mason, P. J., and Arumugam, K., "Free jet scour below dams and flip buckets," Journal of Hydraulic Engineering, ASCE 111, 220 (1985).

Mih, W., "Equations for axisymmetric and two-dimensional turbulent jets," Journal of Hydraulic Engineering, ASCE 115(12), 1715-1719 (1989).

Mueller, R., and Eggenberger, W., "Experimentelle und theoretische Untersuchungen uber das Kolkproblem." Mitt. Versuchanstalt Wasserbau, No. 5, ETH, Zurich (1944). (In German.)

Pagliara, S., and Palermo, M., "Scour control and surface sediment distribution downstream of block ramps," Journal of Hydraulic Research, IAHR 46 (3), 334-343 (2008).

Pagliara, S., and Palermo M., "Influence of tailwater depth and pile position on scour downstream of block ramps," Journal of Irrigation and Drainage Engineering, ASCE 136(2), 120-130 (2010).

Pagliara, S., Hager, W. H., and Minor, H. E., "Hydraulics of plane plunge pool scour," Journal of Hydraulic Engineering, ASCE 132(5), 450-461 (2006).

Pagliara, S., Hager, W. H., and Unger, J., "Temporal evolution of plunge pool scour," Journal of Hydraulic Engineering, ASCE 134(11), 1630-1630 (2008a).

Pagliara, S., Amidei, M., Hager, W. H., "Hydraulics of 3D plunge pool scour," Journal of Hydraulic Engineering, ASCE 134(9), 1275-1284 (2008b).

Parker, G., *1D sediment transport morphodynamics with applications to rivers and turbidity currents*, e-book downloadable at: http://cee.uiuc.edu/people/parkerg/morphodynamics_ebook.htm

Pope, S. B., *Turbulent Flows* (Cambridge Univ. Press, New York, 2000).

Raudkivi, A. J., *Loose Boundary Hydraulics* (Balkema, Rotterdam, 1998).

Rouse, H., "Criteria for similarity in the transportation of sediment," in Proc. 1st Hydraulic Conference, State University of Iowa, Iowa City, Iowa, 33-49 (1940).

Saddoughi, S. G., and Veeravalli, S. V., "Local isotropy turbulent boundary layers at high Reynolds number," Journal of Fluid Mechanics 268, 333–372 (1994).

Shields, A. F., *Anwendung der Ahnlichkeitsmechanik und der Turbulentzforschung auf die Geshiebebewegung* (Mitt. Preuss. Versuchsanst. Wasserbau Schiffbau, Vol. 26, 26 pp., 1936). (English translation by W. P. Ott & J. C. van Uchelen, 1936. Rep. 167, 36 pp., California Institute of Technology, Pasadena. In German.)

Schoklitsch, A., "Kolkbildung unter Uberfallstrahlen," Wasserwirtschaft 343 (1932). (In German.)

Stein, O. R., Julien, P. Y., and Alonso, C. V., "Mechanics of jet scour downstream of a headcut," Journal of Hydraulic Research 31(6), 723-738 (1993).

USGS, Glossary of Glacier Terminology – Text version, http://pubs.usgs.gov/of/2004/1216/text.html#c

Veronese, A., *Erosion of a bed downstream from an outlet*, Colorado A & M College, Fort Collins, United States (1937).

Wilson, L., Ghatan, G. J., Head, J. W., Mitchell, K. L., "Mars outflow channels: A reappraisal of the estimation of water flow velocities from water depths, regional slopes, and channel floor properties," Journal of Geophysical Research 109, E09003 (2004).

Yalin, M. S., *The mechanics of sediment transport* (Pergamon Press, Oxford, 1977).

Table captions

Table 1: Sets of values of the exponents of Eq. (1) empirically determined (or set to zero) by different researchers. Partially adapted from Mason and Arumugam (1985) and Hoffmans and Verheij (1997). Also shown are the theoretical values of the exponents determined from the equilibrium theory detailed in the text and published elsewhere.

Table 2: Laboratory tests analyzed in this paper, both taken from previous research by the authors and especially developed for this work.

Table 3: Laboratory tests especially conducted for this work.

Table 4: Scour depth time evolution for tests with vertical jet (90°).

Table 1: Sets of values of the exponents of Eq. (1) empirically determined (or set to zero) by different researchers. Partially adapted from Mason and Arumugam (1985) and Hoffmans and Verheij (1997). Also shown are the theoretical values of the exponents determined from the equilibrium theory detailed in the text and published elsewhere.

		Exponent				
	Reference	e_q	e_h	e_g	e_d	e_ρ
2D	Schoklitsch (1932)	0.57	0.2	0	-0.32	0
	Veronese (1937)	0.54	0.225	0	-0.42	0
	Muller and Eggenberger (1944)	0.6	0.5	-0.3	-0.4	4/9
	Hartung (1959)	0.64	0.36	0	-0.32	0
	Franke (1960)	0.67	0.5	0	-0.5	0
	Kotoulas (1967)	0.7	0.35	-0.35	-0.4	0
	Chee and Padiyar (1969)	0.67	0.18	0	-0.063	0
	Chee and Kung (1974)	0.6	0.2	0	-0.1	0
	Machado (1980)	0.5	0.3145	0	-0.0645	0
	Bormann and Julien (1991)	0.6	0.5	-0.3	-0.4	0.8
	Hoffmans (1998) (for d_{90}>0.0125 m)	0.5	0.25	-0.25	0	0
	Theory (Bombardelli and Gioia, 2005; Gioia and Bombardelli, 2005)	2/3	2/3	-1/3	-2/3	1
3D	Aderibigbe and Rajaratnam (1996)	0.5	0.25	-0.25	-0.5	0.5
	Abt et al. (1984)	0.345	0.1425	-0.17	0	0
	Theory (Bombardelli and Gioia, 2006)	0.4	0.4	-0.2	-0.4	0.6

Table 2: Laboratory tests analyzed in this paper, both taken from previous research by the authors and especially developed for this work.

Authors	Configuration	Width of channel [m]	Sediment size, d_{50} [mm]	Jet angles	Number of tests
Pagliara et al. (2006)	Nearly 3D. Equilibrium	0.5	6.5	45°, 60°, 90°	37
Pagliara et al. (2008a)	2D* and **/3D**. Evolution	0.5	1.15	45°, 60°	22
Pagliara et al. (2008b)	3D. Equilibrium	0.8	10.3	45°, 60°	89
Pagliara and Palermo (2008)	2D. Equilibrium	0.2	9.5	45°, 60°, 75°, 85°	16
Present study	2D. Equilibrium	0.2	9.5	45°, 60°, 75°, 85°	12
Present study	3D**. Evolution	0.8	7.45	90°	6

Note: *"full model"; **half model "Half model" refers a flow condition in which a symmetry plane was used to simplify the model, and a smaller jet nozzle was employed. In the "full model," i.e., the full jet, no simplification was used.

Table 3: Laboratory tests especially conducted for this work.

Test	Q [l/s]	D [cm]	Δ_{max} [cm]	v_{jet} [m/s]	D_{test} [m]	α [deg]	d_{50} [mm]	ρ_s [kg/m^3]	Config.
1**	3.45	18.9	17	6.03	0.027	90	7.45	2468	3D Evolution
2**	3.45	9.45	16	6.03					
3**	3.45	2.7	15.5	6.03					
4**	2.35	18.9	11	4.11					
5**	2.38	9.45	11	4.16					
6**	2.4	2.7	11	4.19					
7*	2.5	14.3	8.5	4.37		45	9.50	2453	2D Equil.
8*	4.4	14.3	17.3	7.69					
9*	2.5	2.7	8.6	4.37					
10*	2.5	2.8	6.7	4.37		60	9.50	2453	2D Equil.
11*	2.5	18.9	9.7	4.37					
12*	3.5	2.6	13	6.12					
13*	3.5	18.9	16.7	6.12		75	9.50	2453	2D Equil.
14*	4.4	18.9	23.3	7.69					
15*	2.5	13.5	11.1	4.37					
16*	2.5	13.5	9.5	4.37		85	9.50	2453	2D Equil.
17*	3.5	13.5	16.2	6.12					
18*	4.4	13.5	24.9	7.69					

Note: The duration of all tests was of approximately one hour. *"full model;" and **"half model."
All tests were developed for unsubmerged conditions and no aeration of the jet was included.
$D_{test} = D^*$ for "full model."
$D_{test} = D^*/\sqrt{2}$ for "half model."
Q indicates the discharge of the test.

Table 4: Scour depth time evolution for tests with vertical jet (90°).

Test	1**	2**	3**	4**	5**	6**
time [*s*]	*Δ(t)* [*m*]	*Δ(t)* [*m*]	*Δ(t)* [*m*]	*Δ(t)* [*m*]	*Δ(t)* [*m*]	*Δ(t)* [*m*]
0	0	0	0	0	0	0
1	0.070	0.110	0.110	0.040	0.050	0.070
2	0.100	0.130	0.130	0.050	0.055	0.075
3	0.105	0.130	0.135	0.060	0.070	0.080
4	0.110	0.130	0.140	0.065	0.080	0.085
5	0.130	0.135	0.140	0.070	0.080	0.095
6	0.135	0.130	0.145	0.075	0.085	0.095
7	0.140	0.135	0.145	0.075	0.085	0.100
8	0.145	0.135	0.150	0.075	0.085	0.100
9	0.145	0.135	0.150	0.075	0.085	0.100
10	0.145	0.135	0.150	0.075	0.095	0.100
20	0.160	0.140	0.145	0.075	0.100	0.100
30	0.160	0.140	0.145	0.080	0.105	0.100
40	0.160	0.145	0.145	0.095	0.110	0.100
50	0.165	0.145	0.145	0.100	0.110	0.105
60	0.160	0.145	0.145	0.100	0.110	0.105
120	0.170	0.145	0.145	0.100	0.110	0.105
240	0.170	0.150	0.150	0.105	0.110	0.105
480	0.170	0.150	0.150	0.105	0.110	0.105
600	0.170	0.155	0.155	0.105	0.110	0.110
900	0.170	0.155	0.155	0.105	0.110	0.110
1200	0.170	0.155	0.155	0.105	0.110	0.110
1500	0.170	0.155	0.155	0.105	0.110	0.110
1800	0.170	0.160	0.155	0.110	0.110	0.110
2100	0.170	0.160	0.155	0.110	0.110	0.110
2400	0.170	0.160	0.155	0.110	0.110	0.110
3000	0.170	0.160	0.155	0.110	0.110	0.110
3600	0.170	0.160	0.155	0.110	0.110	0.110

Note: **half model

Figure captions

FIG. 1. (a) Sketch of the jet-driven configuration detailing the main hydraulic and geometric parameters. Δ is the time-dependent scour depth; D is the uniform water depth before the scour starts; q indicates the volumetric flow rate in a three-dimensional (3D) set-up (Q_{jet}), or the volumetric flow rate per unit width in a two-dimensional (2D) set-up; α is the jet angle; D^* is the equivalent pipe diameter; and $R = \Delta + D$. Whereas the 2D configuration is "cylindrical," the 3D counterpart is axisymmetric. (b) Picture of the experimental set-up for a 3D configuration.

FIG. 2. (a) Snapshot of the scour evolution process for a test pertaining to a 2D case, a jet angle of 60° and unsubmerged conditions. Solid line indicates the location of the initial granular bed, and flow is from right to left. (b) Detail of the equilibrium scour pothole obtained with a 3D configuration (contours in centimeters with respect to the initial bed elevation) and a jet angle of 60°. Upper tile: Contour map; lower tile: three-dimensional view.

FIG. 3. Schematic of the time evolution of the scour process for the *developing* ((a)-(c)) and *developed* ((d)-(f)) phases. Arrow indicates the direction of the jet, and dots indicate sediment particles in suspension. The inclination of the downstream dune follows the angle of repose.

FIG. 4. Developing phase of the scour process for *coarser* material (flow from right to left). The jet angle is 45° and the configuration is 3D. (a) t=1 s (impact of the jet on the bed material); (b) t=4 s (sediment transport directed both longitudinally and laterally); (c) t=14 s (upstream ridge surface is fully developed); (d) t=25 s, end of the developing phase (both upstream and downstream surfaces of the ridge are fully developed). Test undertaken for this work.

FIG. 5. Developed phase of the scour process for *coarser* material (flow from left to right). The jet angle is 60° and the configuration is 3D. In (a) and (b), the expansion of the scour hole is depicted (t=300 s and t=600 s, respectively) and in (c) the dynamic equilibrium configuration is shown (t=3600 s); (d) static equilibrium configuration. Test undertaken for this work.

FIG. 6. Pothole behavior during the developing phase for 90°. Scour evolution for Test 5 (see Table 4) at: (a) t=4 s, (b) t=5 s (scour hole enlargement with almost the same scour depth of t=4 s); t=6 s (increase of the scour depth), (d) t=7 (scour hole enlargement with almost the same scour depth of t=6 s).

FIG. 7. Time evolution of the scour depth for 3D tests with jet angle equal to 90°, along with the plots of the lines indicating the transition between developing and developed phases for 90° (this study) and 45° and 60° (derived from Pagliara et al. 2008a). The scour depth has been made non-dimensional with the equivalent jet diameter.

FIG. 8. Developing phase of the scour process for *coarser* material and a jet angle of 90° in 3D (Test 1 undertaken for this paper): (a) t=1 s (impact of the jet on the bed material); (b) t=3 s (development of both upstream and downstream surface of the ridge); (c) t=9 s (further development of both upstream and downstream surface of the ridge); (d) t=12 s, end of the developing phase (both upstream and downstream surface of the ridge are fully developed).

FIG. 9. Developed phase of the scour process for *coarser* material and a jet angle of 90° in 3D (Test 1 undertaken for this paper): (a), (b) and (c) slight expansion of the scour hole (t=60 s, 120 s, and t=180 s, respectively); (d) static configuration.

FIG. 10. Developing phase of the scour process for *fine* material, a jet angle of 45° and a 2D configuration (flow from left to right). (a) t=1.5 s (impact of the jet on the bed material); (b) t=3 s (sediment transport directed longitudinally); (c) t=40 s (upstream ridge surface fully developed); (d) t=75 s, end of the developing phase (both upstream and downstream surface of the ridge are fully developed). Test undertaken in 2008; unpublished papers.

FIG. 11. Developed phase of the scour process for *fine* material, a jet angle of 45° and a 2D configuration (flow from left to right). (a) and (b) expansion of the scour hole (t=3200 s and t=3900 s, respectively); (c) dynamic equilibrium configuration (t=7000 s); (d) static equilibrium configuration. Test undertaken in 2008; unpublished papers.

FIG. 12. Time evolution of the scour process for different jet angles: (a) α=30°; (b) α=45°; (c) α=60° (data from Pagliara et al. 2008a); and (d) α=90° (present study). The vertical dotted line represents the transition developing/developed phase. The nomenclature of the tests, developed in Zurich, follows that of Pagliara et al. (2008a). The first number indicates the test number; after the A, the angle is indicated; finally "S" or "U" indicates submerged or unsubmerged conditions.

FIG. 13. (a) Sketch of the turbulent cauldron with its largest eddies of characteristic velocity V (left side), three grains of diameter d lying on the surface of the pothole, along with the fluctuating velocities normal and tangent to the wetted surface S (v_n and v_t, respectively), and u_d indicating the velocity scale of eddies of size d (adapted from

Bombardelli and Gioia 2006) (right side); (b) sketch of the adopted pothole geometry for the evolution of the scour process at any given time.

FIG. 14. Determination of the multiplicative constants in Eqs. (6). In 2D, for the tests of Pagliara and Palermo (2008), the width of the channel was used to compute the discharge per unit width, whereas the equivalent pipe diameter was used to that end for tests by Pagliara et al. (2008a). This decision was made based on images and videos of the tests.

FIG. 15. Comparison among measured and predicted values (Eq. 6b) for all data from Veronese (1937). Depths are expressed in meters.

FIG. 16. Numerical solutions of Eq. (11) for the 2D configuration and a jet angle of 45°, and comparison against experimental data. (a) Calibration (data from Pagliara et al. 2008a). (b) Validation (data from Pagliara et al. 2008a).

FIG. 17. Numerical solutions of Eq. (11) for the 2D configuration and a jet angle of 60°, and comparison against experimental data from Pagliara et al. (2008a).

FIG. 18. Numerical solutions of Eq. (14) for the 3D configuration and a jet angle of 45°, and comparison against experimental data. (a) Calibration (data from Pagliara et al. 2008a). (b) Validation (data from Pagliara et al. 2008a).

FIG. 19. Numerical solutions of Eq. (14) for the 3D configuration and a jet angle of 90°, and comparison against experimental data from present study.

FIG. 20. Comparison among measured and predicted values (Eqs. (11) and (14)) for the time evolution of the scour depth. Depths are expressed in meters.

FIG. 21. Validation of model predictions against data pertaining to the case of Run 22 of Stein et al. (1993).

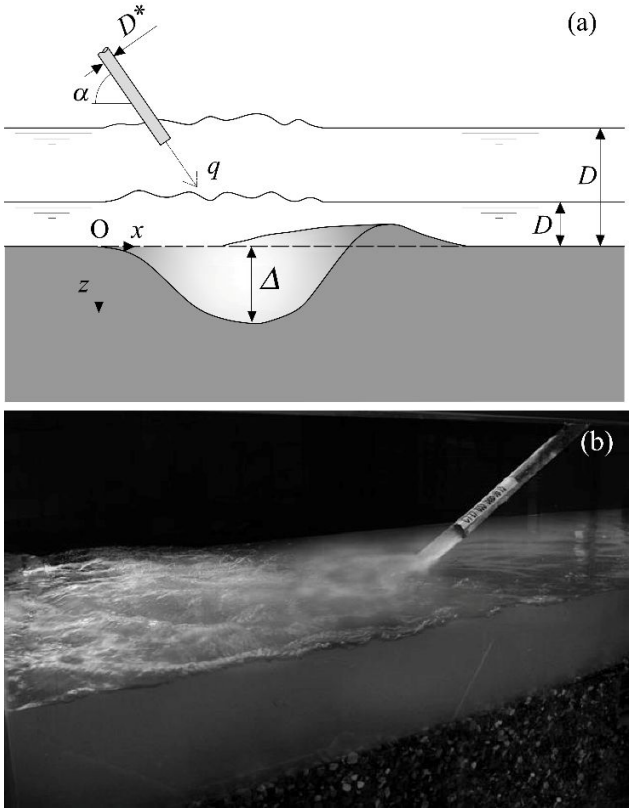

FIG. 1. (a) Sketch of the jet-driven configuration detailing the main hydraulic and geometric parameters. Δ is the time-dependent scour depth; D is the uniform water depth before the scour starts; q indicates the volumetric flow rate in a three-dimensional (3D) set-up (Q_{jet}), or the volumetric flow rate per unit width in a two-dimensional (2D) set-up; α is the jet angle; D^* is the equivalent pipe diameter; and $R = \Delta + D$. Whereas the 2D configuration is "cylindrical," the 3D counterpart is axisymmetric. (b) Picture of the experimental set-up for a 3D configuration.

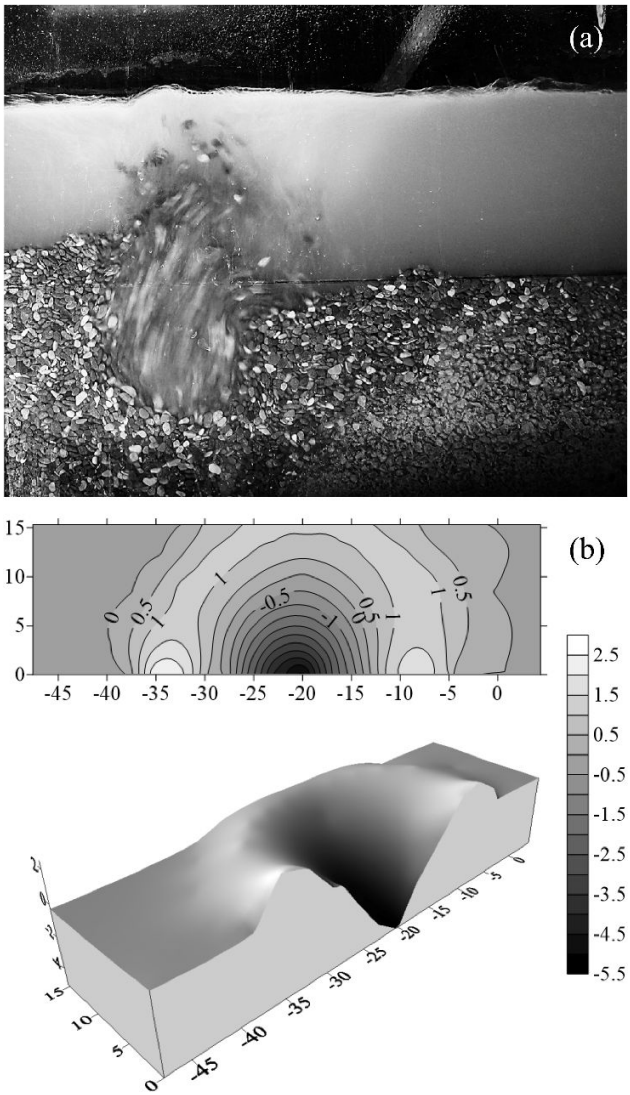

FIG. 2. (a) Snapshot of the scour evolution process for a test pertaining to a 2D case, a jet angle of 60° and unsubmerged conditions. Solid line indicates the location of the initial granular bed, and flow is from right to left. (b) Detail of the equilibrium scour pothole obtained with a 3D configuration (contours in centimeters with respect to the initial bed elevation) and a jet angle of 60°. Upper tile: Contour map; lower tile: three-dimensional view.

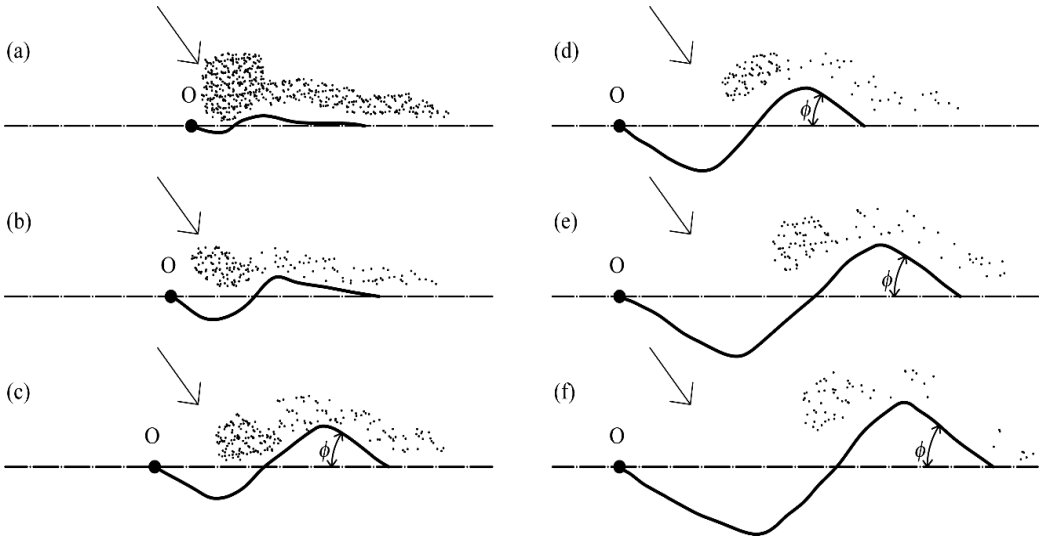

FIG. 3. Schematic of the time evolution of the scour process for the *developing* ((a)-(c)) and *developed* ((d)-(f)) phases. Arrow indicates the direction of the jet, and dots indicate sediment particles in suspension. The inclination of the downstream dune follows the angle of repose.

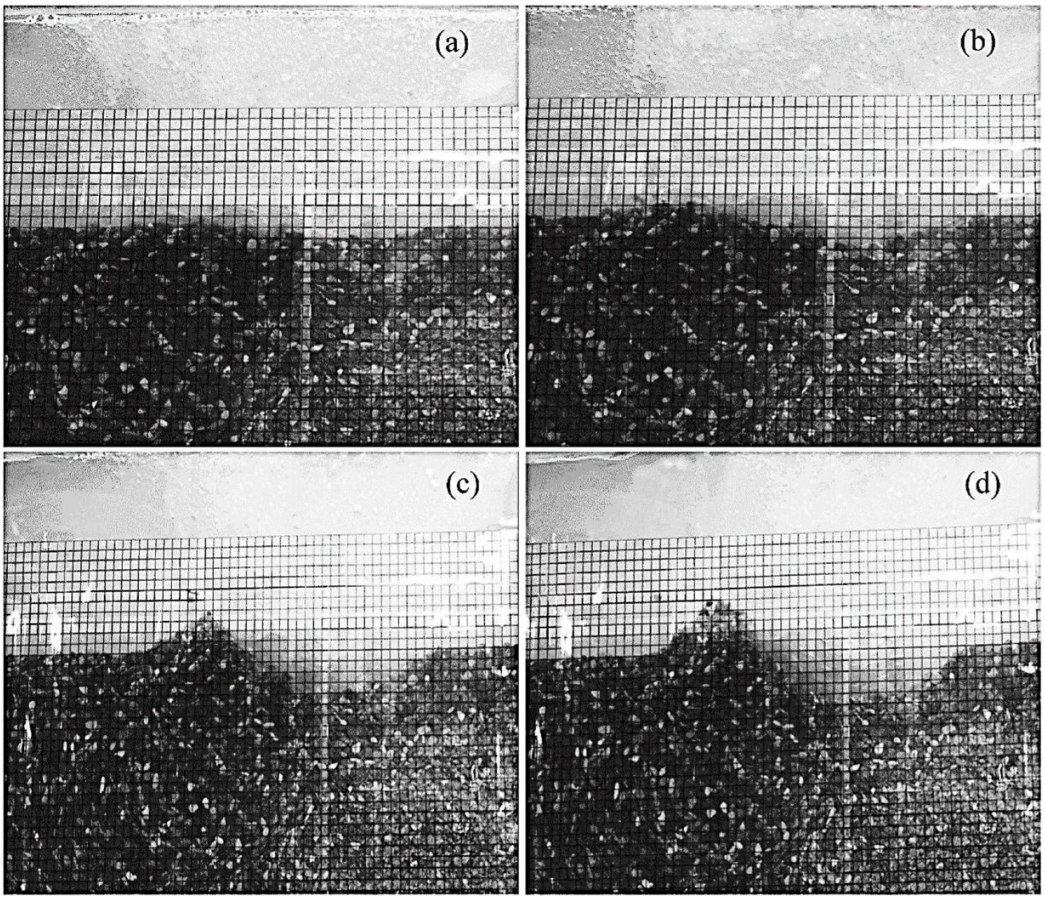

FIG. 4. Developing phase of the scour process for *coarser* material (flow from right to left). The jet angle is 45° and the configuration is 3D. (a) t=1 s (impact of the jet on the bed material); (b) t=4 s (sediment transport directed both longitudinally and laterally); (c) t=14 s (upstream ridge surface is fully developed); (d) t=25 s, end of the developing phase (both upstream and downstream surfaces of the ridge are fully developed). Test undertaken for this work.

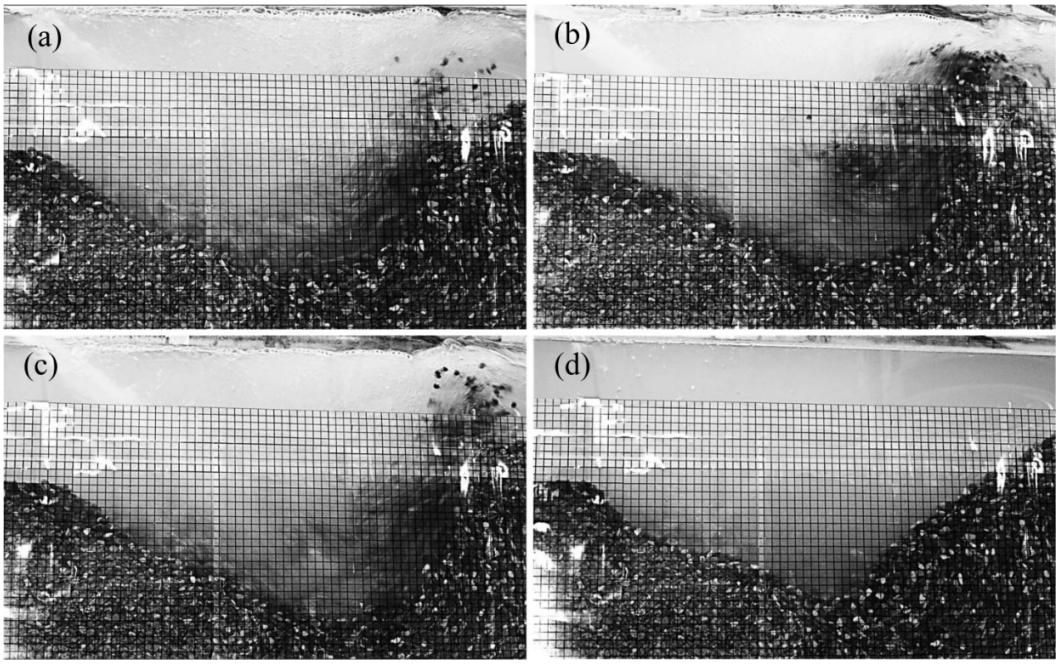

FIG. 5. Developed phase of the scour process for *coarser* material (flow from left to right). The jet angle is 60° and the configuration is 3D. In (a) and (b), the expansion of the scour hole is depicted (t=300 s and t=600 s, respectively) and in (c) the dynamic equilibrium configuration is shown (t=3600 s); (d) static equilibrium configuration. Test undertaken for this work.

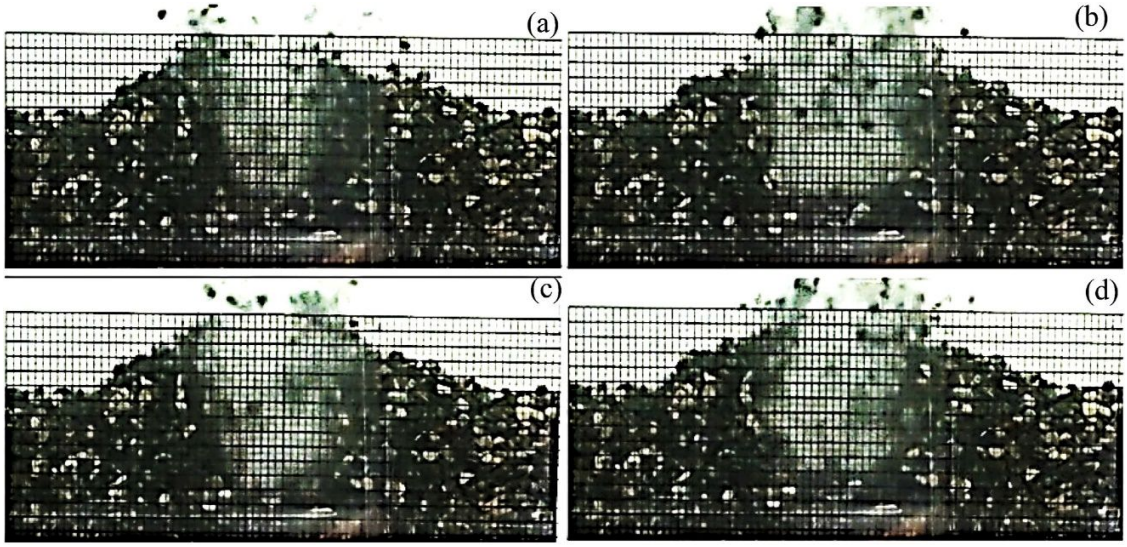

FIG. 6. Pothole behavior during the developing phase for 90°. Scour evolution for Test 5 (see Table 4) at: (a) t=4 s, (b) t=5 s (scour hole enlargement with almost the same scour depth of t=4 s); t=6 s (increase of the scour depth), (d) t=7 (scour hole enlargement with almost the same scour depth of t=6 s).

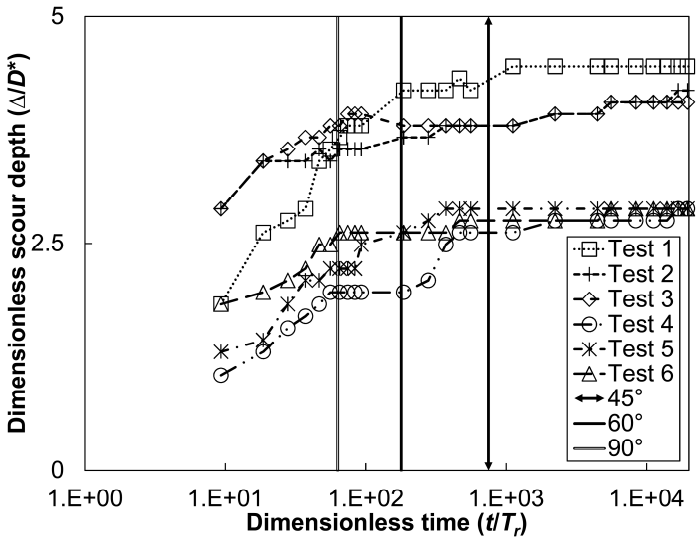

FIG. 7. Time evolution of the scour depth for 3D tests with jet angle equal to 90°, along with the plots of the lines indicating the transition between developing and developed phases for 90° (this study) and 45° and 60° (derived from Pagliara et al. 2008a). The scour depth has been made non-dimensional with the equivalent jet diameter.

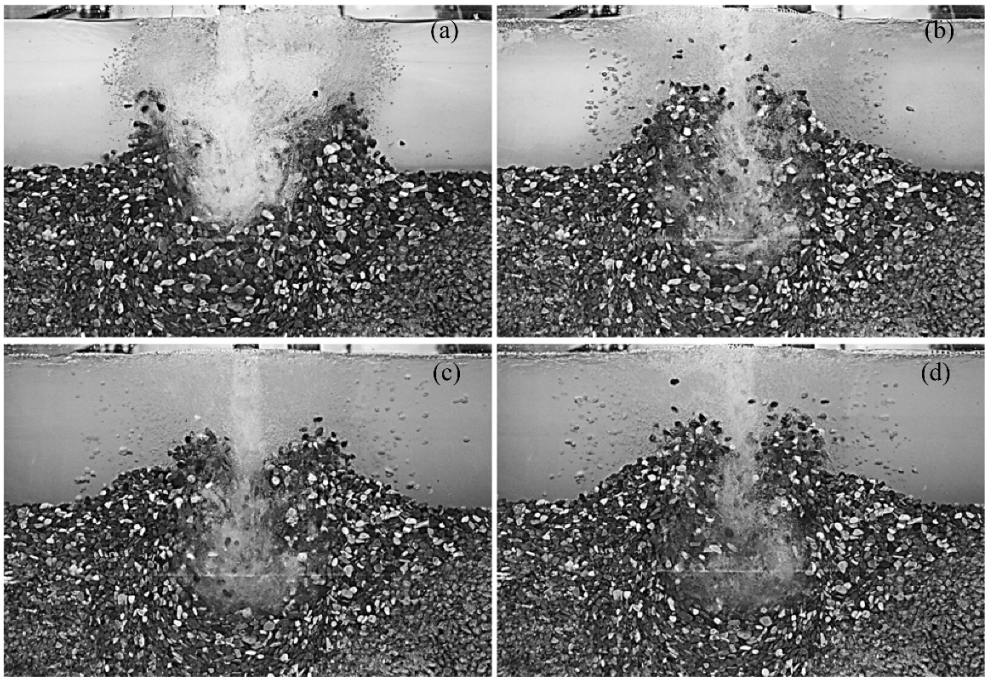

FIG. 8. Developing phase of the scour process for *coarser* material and a jet angle of 90° in 3D (Test 1 undertaken for this paper): (a) t=1 s (impact of the jet on the bed material); (b) t=3 s (development of both upstream and downstream surface of the ridge); (c) t=9 s (further development of both upstream and downstream surface of the ridge); (d) t=12 s, end of the developing phase (both upstream and downstream surface of the ridge are fully developed).

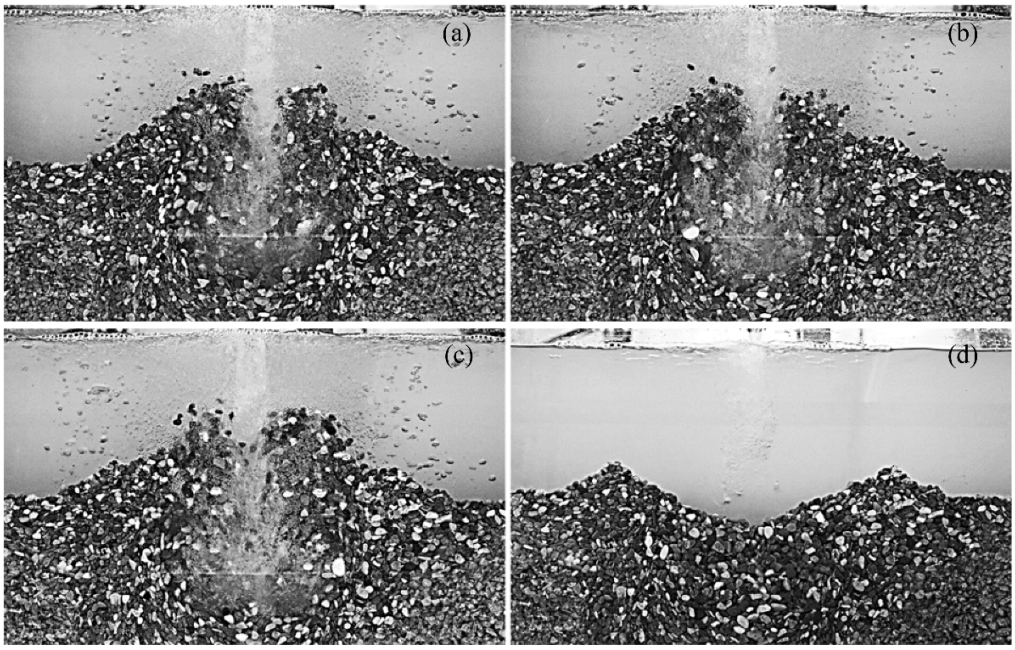

FIG. 9. Developed phase of the scour process for *coarser* material and a jet angle of 90° in 3D (Test 1 undertaken for this paper): (a), (b) and (c) slight expansion of the scour hole (t=60 s, 120 s, and t=180 s, respectively); (d) static configuration.

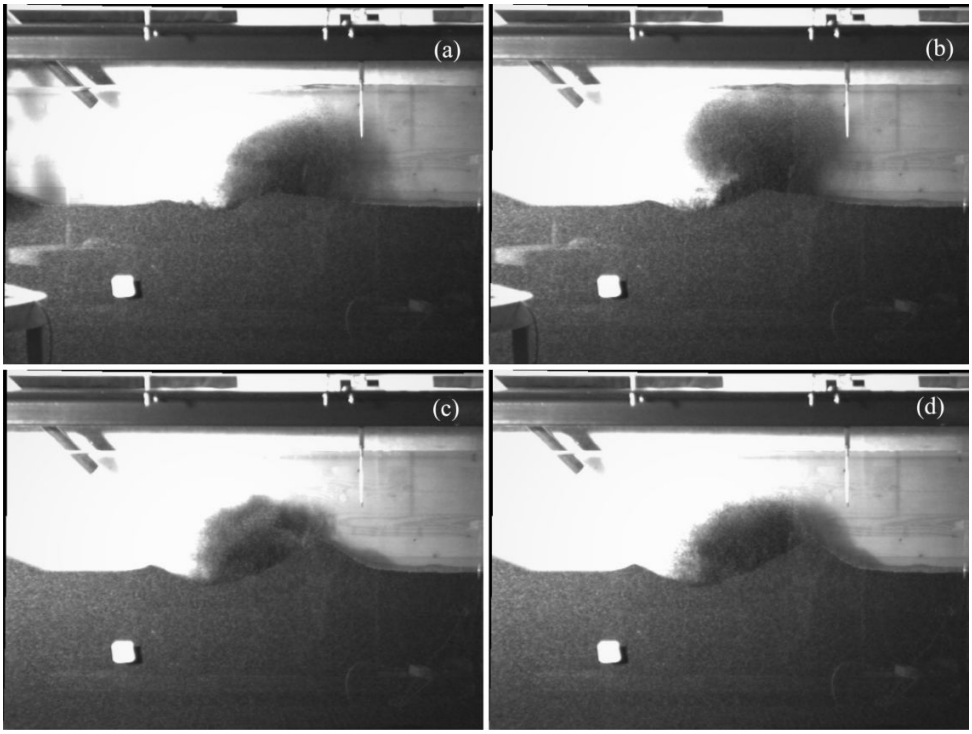

FIG. 10. Developing phase of the scour process for *fine* material, a jet angle of 45° and a 2D configuration (flow from left to right). (a) t=1.5 s (impact of the jet on the bed material); (b) t=3 s (sediment transport directed longitudinally); (c) t=40 s (upstream ridge surface fully developed); (d) t=75 s, end of the developing phase (both upstream and downstream surface of the ridge are fully developed). Test undertaken in 2008; unpublished papers.

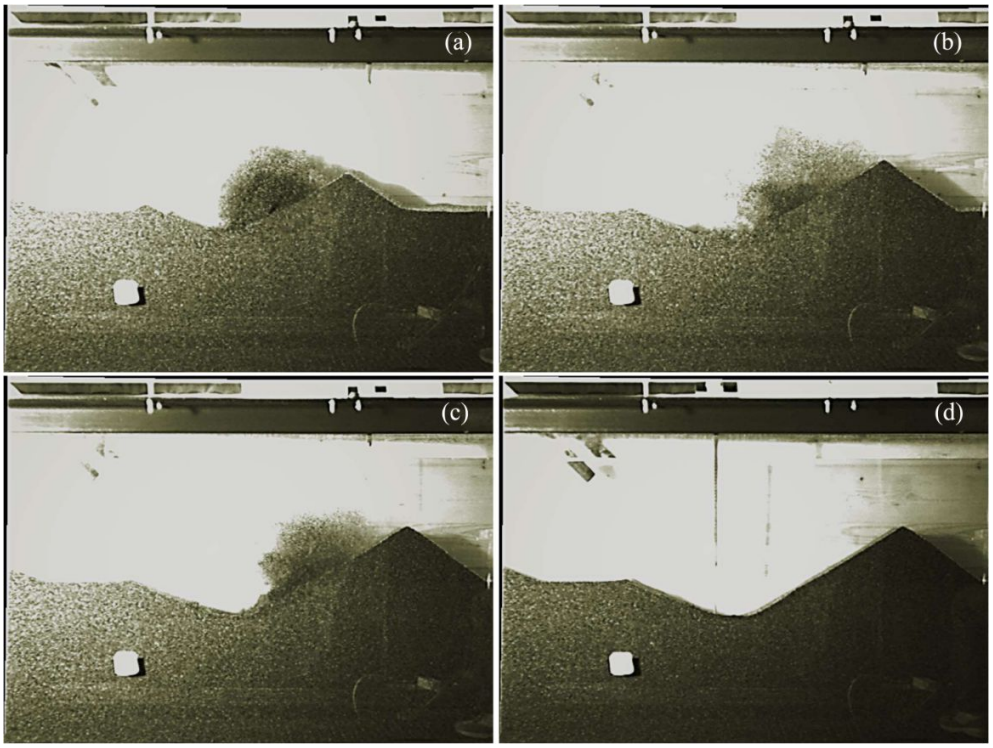

FIG. 11. Developed phase of the scour process for *fine* material, a jet angle of 45° and a 2D configuration (flow from left to right). (a) and (b) expansion of the scour hole (t=3200 s and t=3900 s, respectively); (c) dynamic equilibrium configuration (t=7000 s); (d) static equilibrium configuration. Test undertaken in 2008; unpublished papers.

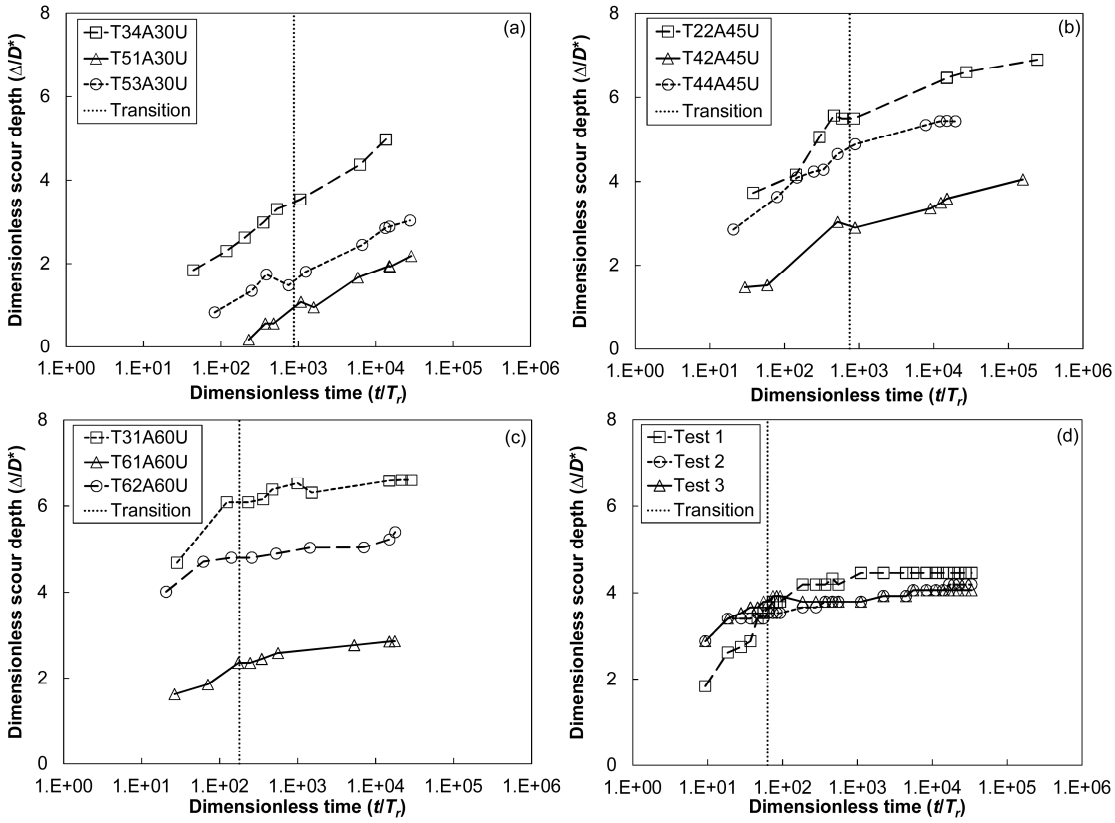

FIG. 12. Time evolution of the scour process for different jet angles: (a) α=30°; (b) α=45°; (c) α=60° (data from Pagliara et al. 2008a); and (d) α=90° (present study). The vertical dotted line represents the transition developing/developed phase. The nomenclature of the tests, developed in Zurich, follows that of Pagliara et al. (2008a). The first number indicates the test number; after the A, the angle is indicated; finally "S" or "U" indicates submerged or unsubmerged conditions.

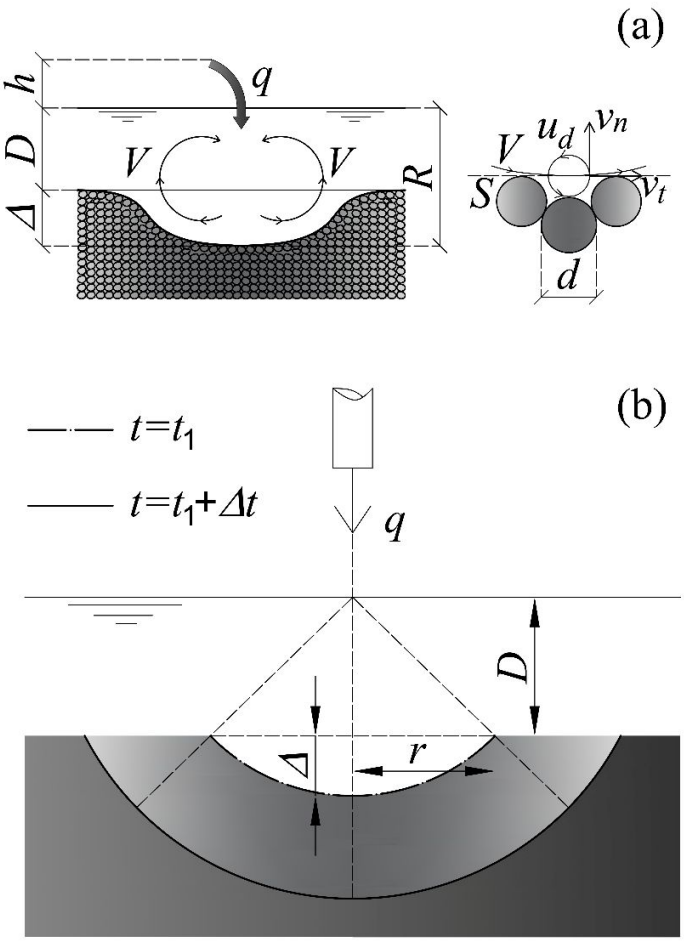

FIG. 13. (a) Sketch of the turbulent cauldron with its largest eddies of characteristic velocity V (left side), three grains of diameter d lying on the surface of the pothole, along with the fluctuating velocities normal and tangent to the wetted surface S (v_n and v_t, respectively), and u_d indicating the velocity scale of eddies of size d (adapted from Bombardelli and Gioia 2006) (right side); (b) sketch of the adopted pothole geometry for the evolution of the scour process at any given time.

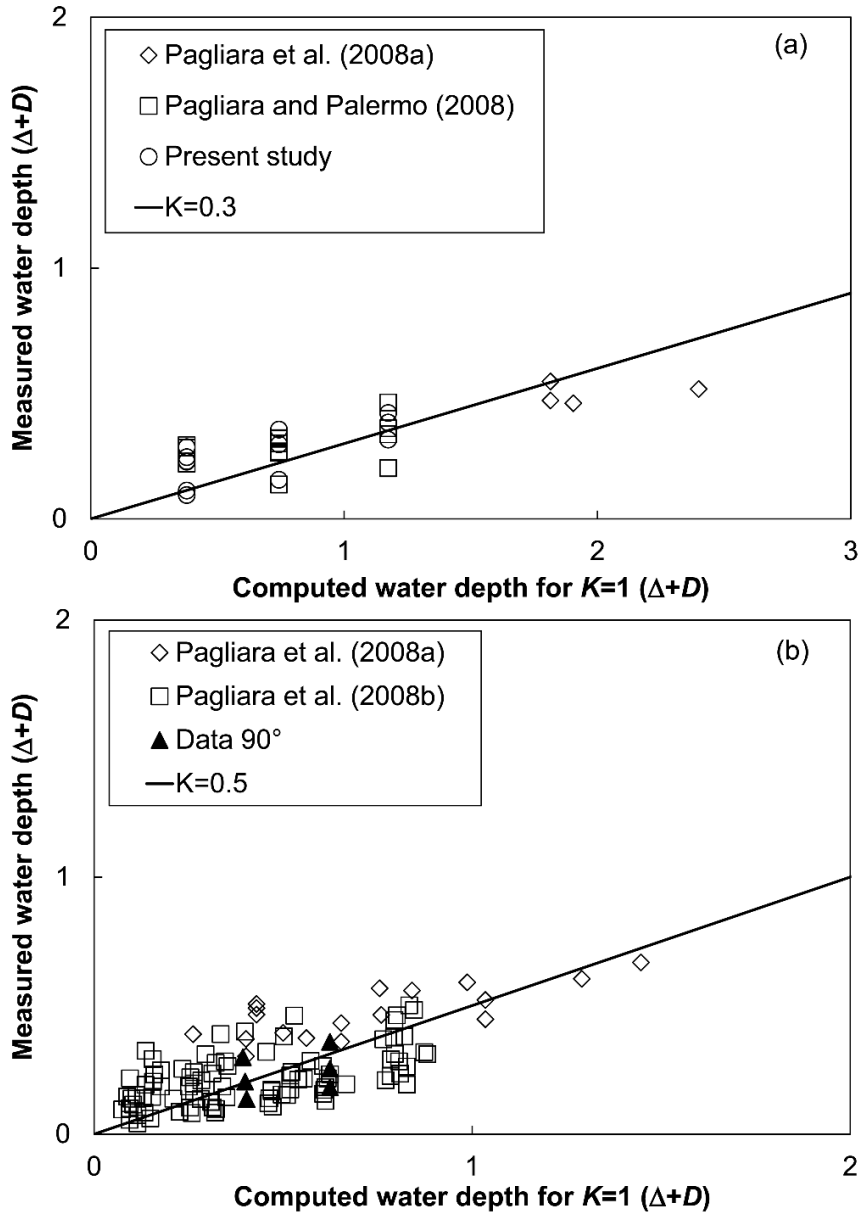

FIG. 14. Determination of the multiplicative constants in Eqs. (6). In 2D, for the tests of Pagliara and Palermo (2008), the width of the channel was used to compute the discharge per unit width, whereas the equivalent pipe diameter was used to that end for tests by Pagliara et al. (2008a). This decision was made based on images and videos of the tests.

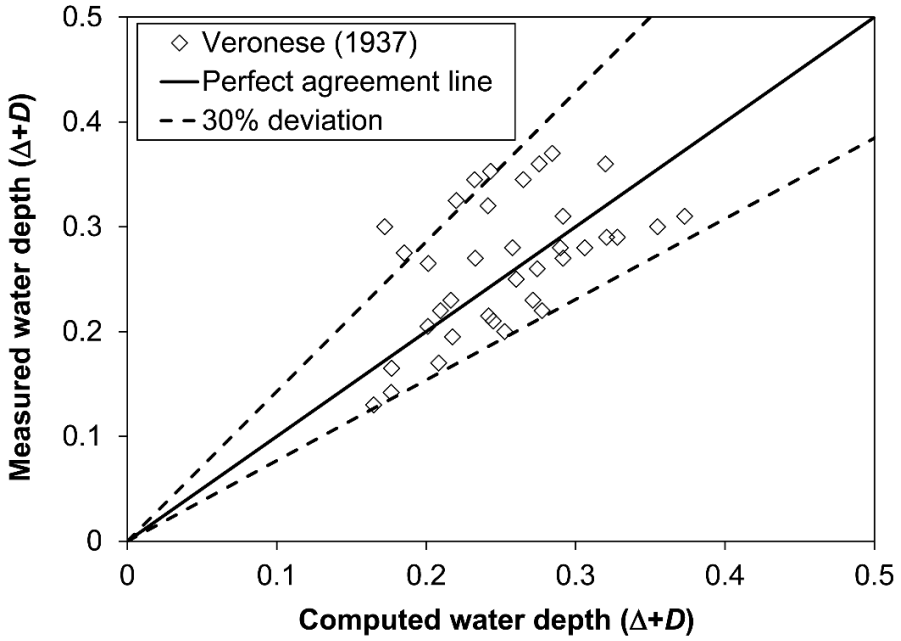

FIG. 15. Comparison among measured and predicted values (Eq. 6b) for all data from Veronese (1937). Depths are expressed in meters.

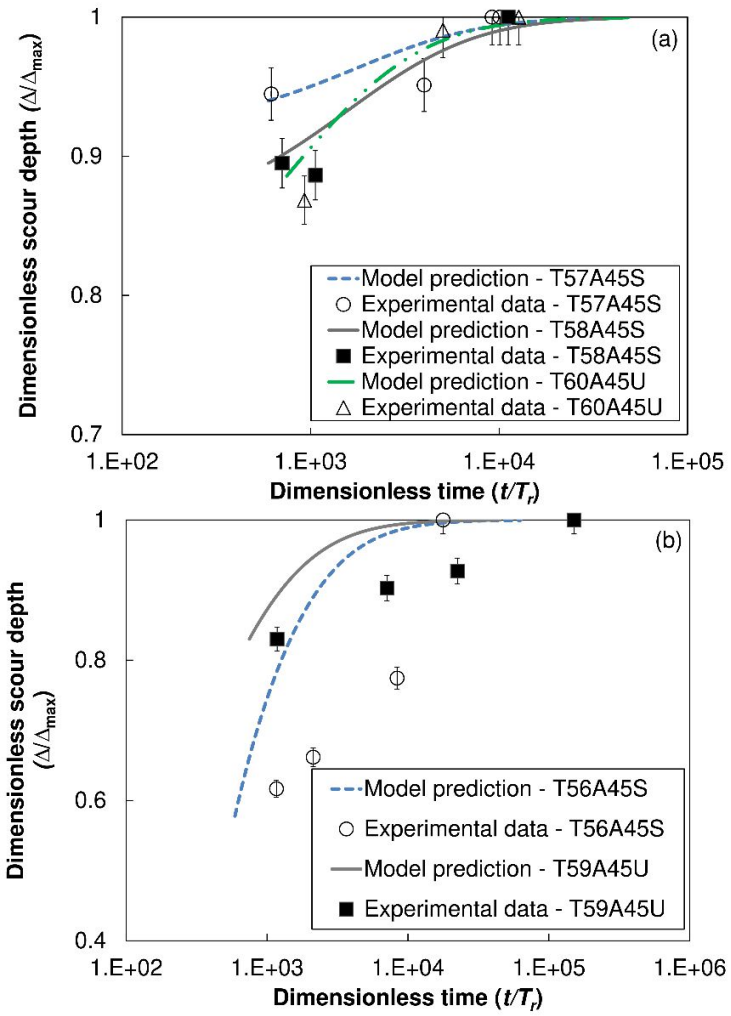

FIG. 16. Numerical solutions of Eq. (11) for the 2D configuration and a jet angle of 45°, and comparison against experimental data. (a) Calibration (data from Pagliara et al. 2008a). (b) Validation (data from Pagliara et al. 2008a).

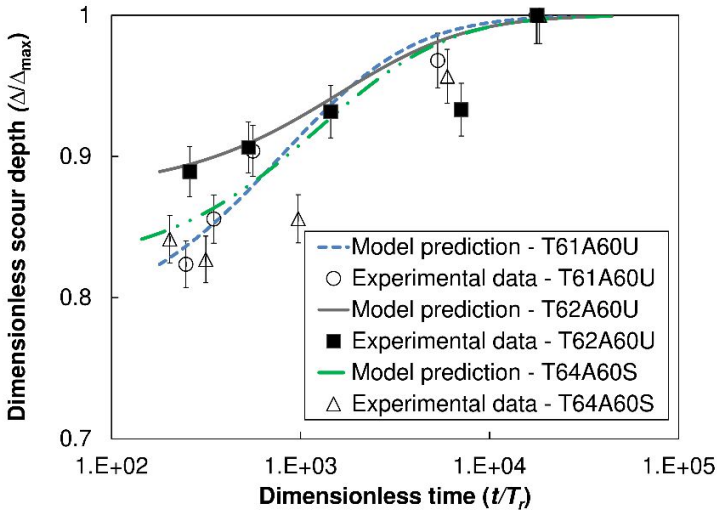

FIG. 17. Numerical solutions of Eq. (11) for the 2D configuration and a jet angle of 60°, and comparison against experimental data from Pagliara et al. (2008a).

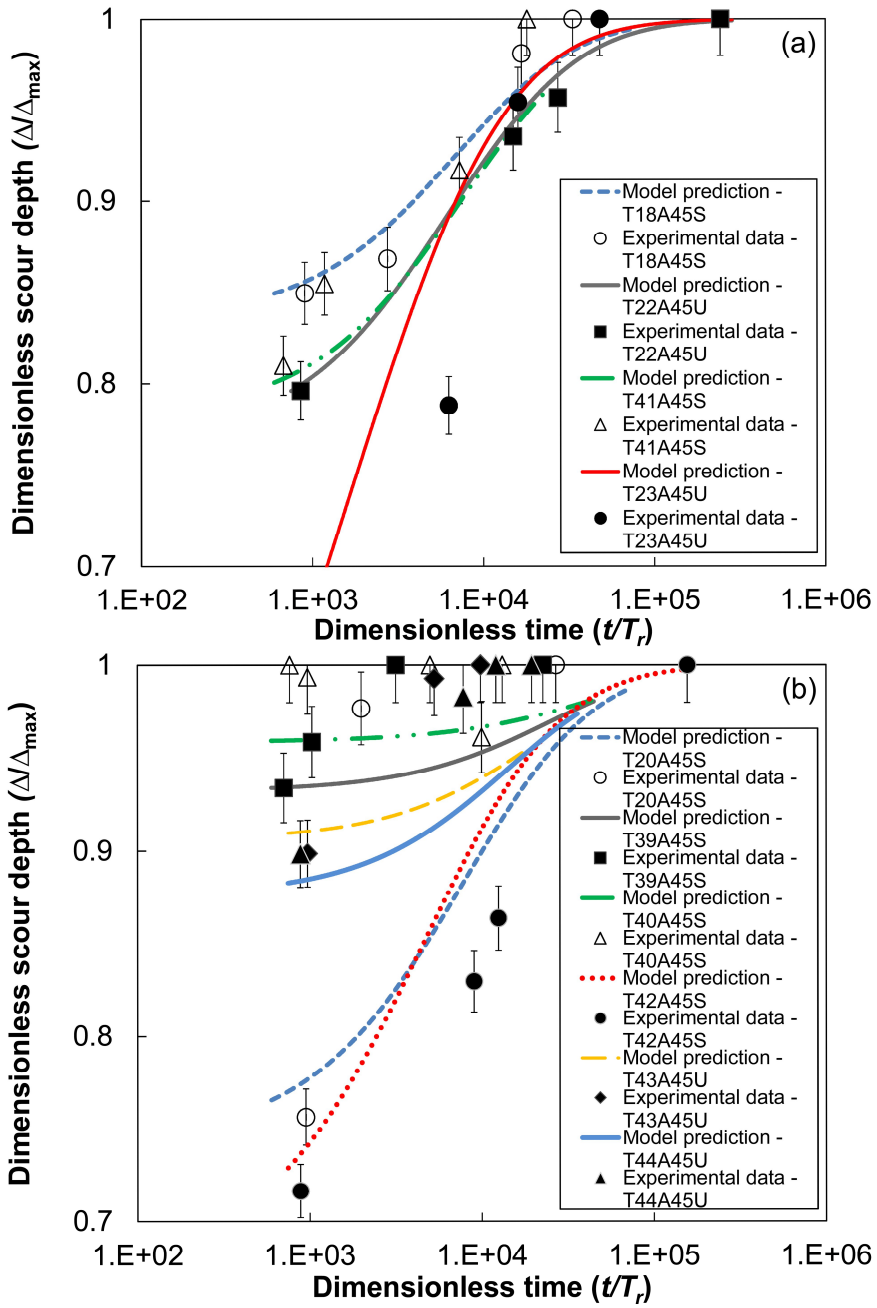

FIG. 18. Numerical solutions of Eq. (14) for the 3D configuration and a jet angle of 45°, and comparison against experimental data. (a) Calibration (data from Pagliara et al. 2008a). (b) Validation (data from Pagliara et al. 2008a).

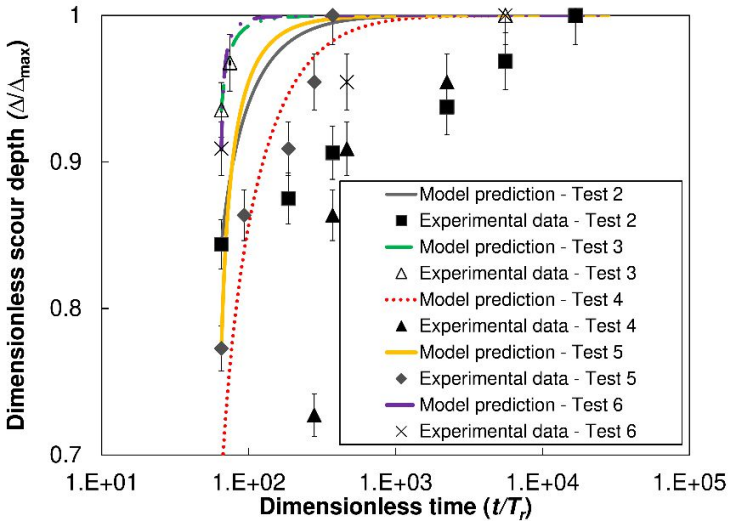

FIG. 19. Numerical solutions of Eq. (14) for the 3D configuration and a jet angle of 90°, and comparison against experimental data from present study.

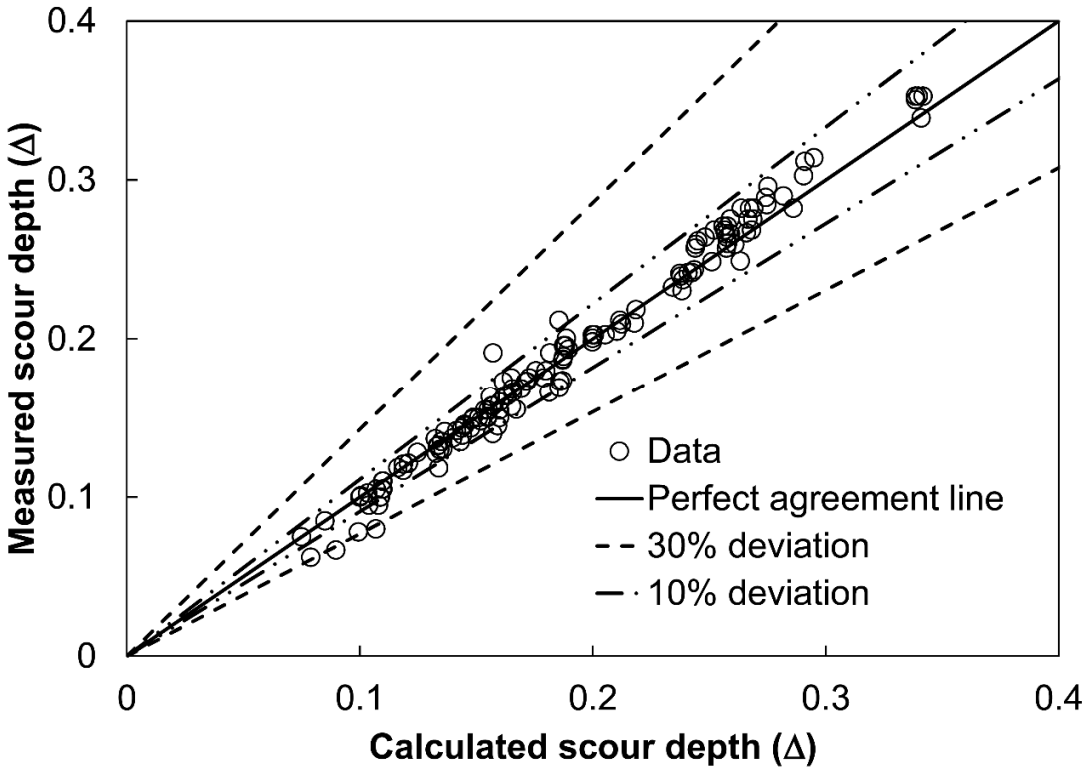

FIG. 20. Comparison among measured and predicted values (Eqs. (11) and (14)) for the time evolution of the scour depth. Depths are expressed in meters.

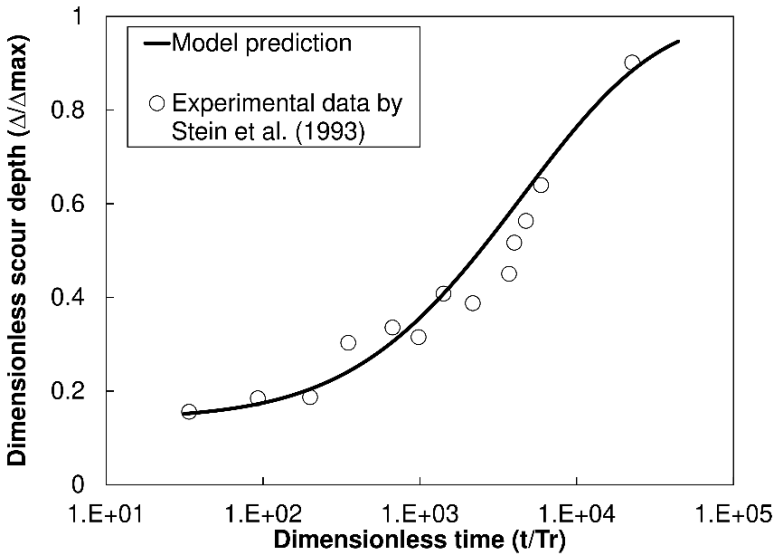

FIG. 21. Validation of model predictions against data pertaining to the case of Run 22 of Stein et al. (1993).